3-22-2019

Global Ionosonde and GPS Radio Occultation Sporadic-E Intensity and Height Comparison

Joshua Y. Gooch

Global Ionosonde and GPS Radio Occultation Sporadic-E Intensity and Height Comparison

THESIS

Joshua Y. Gooch, Capt, USAF

AFIT-ENP-MS-19-M-079

DEPARTMENT OF THE AIR FORCE
AIR UNIVERSITY

AIR FORCE INSTITUTE OF TECHNOLOGY

Wright-Patterson Air Force Base, Ohio

AFIT-ENP-MS-19-M-079

GLOBAL IONOSONDE AND GPS RADIO OCCULTATION SPORADIC-E INTENSITY AND HEIGHT COMPARISON

THESIS

Presented to the Faculty

Department of Engineering Physics

Graduate School of Engineering and Management

Air Force Institute of Technology

Air University

Air Education and Training Command

in Partial Fulfillment of the Requirements for the

Degree of Master of Science in Applied Physics

Joshua Y. Gooch, B.S.

Capt, USAF

21 Mar 2019

AFIT-ENP-MS-19-M-079

GLOBAL IONOSONDE AND GPS RADIO OCCULTATION SPORADIC-E INTENSITY AND HEIGHT COMPARISON

THESIS

Joshua Y. Gooch, B.S.
Capt, USAF

Committee Membership:

Maj D. Emmons, Ph.D.
Chair

Dr. J. Colman
Member

Maj O. Nava, Ph.D.
Member

Abstract

A global, multi-year comparison of low and mid-latitude COSMIC GPS radio occultation (RO) sporadic-E (E_s) plasma frequency and altitude and Digisonde blanketing frequency (fbEs) and altitude within 150 km and 30 minutes of each other. RO methods used to estimate the intensity of the E_s layer include the scintillation index S4, total electron content (TEC) with both a constant and variable E_s cloud thickness, and an Abel transform. The S4 and TEC with varying thickness techniques both under-represent the fbEs values while the TEC with constant thickness and Abel transform better estimate Digisonde fbEs values. All RO methods underestimate the altitude of the fbEs events as measured by the Digisondes. No method outperformed the other techniques across every metric, but the physical basis of the TEC technique provides an advantage over the empirically derived S4. The Abel transform also shows promise, but the lower resolution data currently available is detrimental to its performance. Overall, an automated TEC method tested on a larger data set could prove valuable for real-time global E_s observation.

Acknowledgements

It would have been impossible to complete AFIT without the patience, love and support from my wife. You've always been my biggest supporter, and a constant source of encouragement through this journey.

I would also like to thank my thesis advisor, Maj Dan Emmons, for always challenging me academically and forcing me to become comfortable in the uncomfortable. I have no doubt that these skills you've taught me will help me immensely in my future. I would also like to extend my gratitude to my other committee members, Dr. Jonah Colman and Maj Omar Nava. Both of your insights and critical thinking skills has made me a better scientist and me better understand the scientific challenges facing the Air Force.

Joshua Y. Gooch

Table of Contents

Page

List of Figures

List of Tables

I. Introduction

Abnormal ionospheric conditions cause signal degradation for electromagnetic waves used for long-range and satellite communication, over-the-horizon radar (OTHR) and HF geolocation, sometimes blocking the applications entirely. Real-time global observation of the E-layer of the ionosphere by ground based observing systems is currently limited due to relatively small number of stations. The two main types of ground based ionospheric observation are the ionosonde and incoherent-scatter radar. Both of these methods utilize the reflection of radio signals from the electrons in the ionosphere for characterization of the layers. These ground based systems provide a snapshot of the local ionosphere above the station, but are restricted by the need of large power supplies or antennae arrays.

The Constellation Observing Satellite for Meteorology, Ionosphere, and Climate (COSMIC) offers opportunity for a vast real-time picture of the Earth's atmosphere. Currently, the first iteration of this constellation is nearing its sunset period with its follow-on set for launch in the near future. The COSMIC-2 program will increase the coverage from COSMIC-1 and allow for near real-time observation of the ionosphere. Proper understanding and use of the signal data between the GPS satellite constellation and COSMIC allows for more comprehensive global ionospheric observations.

GPS radio occultation (RO) is a remote sensing technique that analyzes GPS signals measured by low earth orbit (LEO) satellites, such as COSMIC, to determine the conditions along the path. As the signal passes through the atmosphere, it can become distorted by strong gradients along its path. One source of a strong gradient in the ionosphere is sporadic-E (E_s), which is characterized by an abnormal enhancement in the electron density and plasma frequency in the E-layer. These sporadic-E events are caused by the convergence of metallic ions due to wind shear and its interaction with the Earth's magnetic field (Arras, 2010). The accumulation of these heavy

and positively charged ions attract higher densities of electrons leading to enhanced electron densities and consequences to radio signals attempting to penetrate or reflect. Due to lower recombination rates of the metallic ions, these ions are long lived in the Ionosphere (Aikin and Goldberg, 1973; Arras, 2010).

These sporadic-E layers cause scintillation of radio waves used for satellite communications in the Ultra High Frequency (UHF) and Very High Frequency (VHF) bands (Zeng and Sokolovskiy, 2010). Also, they affect radio wave propagation in the HF and lower frequency bands with impacts to OTHR performance inhibiting F-layer propagation (Barnum and Simpson, 1997). Sporadic-E has been proved to be a common occurrence in the mid and low latitudes with many studies demonstrating the occurrence rate and spatial distribution. Sporadic-E events show a maximum in occurrence in the summer hemisphere in the mid to low latitudes (Hocke et al., 2001; Wu et al., 2005). Occurrence rates based on solar cycle have been investigated with no conclusive evidence for dependence on solar maximum of minimum for sporadic-E (Baggaley, 1984; Maksyutin et al., 2001). Though the work done by Maksyutin et al. (2001) demonstrated that during solar max the strength of the layers was increased predominantly due to increased non-metallic ion concentrations.

While many studies have worked to expand GPS radio occultation for a global assessment looking at global occurrence rates of sporadic-E (Arras and Wickert, 2018; Arras et al., 2008; Chu et al., 2014; Hocke et al., 2001; Wickert et al., 2004; Wu et al., 2005; Yeh et al., 2012), few try characterize the intensity and height of these layers against a ground based observation. For example, the analysis by Chu et al. (2014) provides a set of binary requirements for the measurement of a sporadic-E layer from GPS-RO measurements but does not attempt to calculate the strength of the layer. Previous global comparisons of GPS-RO derived foF2 and hmF2 to ionosonde measured values have been performed (Chu et al., 2010), but similar global compar-

isons for sporadic-E are lacking. The Arras and Wickert (2018) study fit GPS-RO sporadic-E S4 and height measurements to Digisonde data collected at Pruhonice, Czech Republic and developed an empirical relationship between the data sets. Similarly, Niu et al. (2015) calculated total electron content (TEC) for the sporadic-E layers and performed a fit to ground-based measurements over Europe. This study aims to perform a global comparison of ionosonde measured sporadic-E intensity and height to GPS-RO measured parameters using several techniques.

Several different methods for converting GPS-RO measurements to electron density have been developed. Hocke et al. (2001) use differences in excess to calculate a TEC and then assume a constant sporadic-E thickness to convert the TEC to an electron density. This assumption of constant thickness does not match observations, and a technique outlined by Zeng and Sokolovskiy (2010) provides a method for estimating sporadic-E layer thickness from GPS-RO observations. This variable thickness technique will be implemented in this study to analyze the effect of intensity calculations using a more realistic thickness to determine the signal path length through the sporadic-E layer. A separate technique uses an Abel transform to convert TEC measurements to electron density for a complete altitude profile (Ahmad, 1998; Hajj and Romans, 1998; Schriener et al., 1999). The empirical relationship between S4 and fbEs outlined in Arras and Wickert (2018) provides an alternative method for estimating sporadic-E intensity. These techniques will be implemented and compared to a set of worldwide ionosonde measurements of sporadic-E to analyze the accuracy of each technique. Overall, the ability of an individual technique to match observations or have a consistent correctable bias would enable extrapolation to a global near real time observation network. A quality GPS radio occultation measurement technique would allow for assimilation into global ionospheric models or verification of current modeling of the E-layer during sporadic-E events.

This document builds an understanding of the structure, important characteristics of the ionosphere, the abnormal E-layer phenomena of sporadic-E, and two measurement methods in Chapter II. Chapter III discusses the development of the ionosonde data set for comparison, as well as the theory and methodology behind the four applied GPS-RO techniques and associated results. Then a comparison between the ionosonde derived heights and intensities with the GPS-RO data is presented. Lastly, Chapter IV provides conclusions and recommendations for future work with this study.

II. Background

The purpose of this chapter is to build a baseline understanding of the physical structure and observation methodologies of the ionosphere. First provided is substantiating information on the basic structure of the standard ionosphere. Second, the measurement parameters used to characterize conditions in the ionosphere are presented along with a description of abnormal variations of those parameters. Third, the methods for measuring conditions in the ionosphere by using ground based ionosondes are outlined. Finally, this chapter describes the background mechanics of how and what GPS radio occultation provides and why it is a quality data source for identification of sporadic-E.

2.1 Ionosphere

The ionosphere is the layer of the atmosphere from about 50 km to 1000 km above the Earth's surface (Pisacane, 2008). At the height of 50km, the distribution of standard constituents in the atmosphere begin to change due to the effects of gravity. Heavier atoms and molecules begin to decrease in concentration more rapidly with increasing altitude. Although neutral particle concentrations are decreasing with altitude there is still absorption of high energy photons from the sun. These photons have energies greater than the ionization potential energies of the particles leading to photoionization; the creation of electron-ion pairs from neutral constituents in the upper atmosphere. In general, the varying concentrations of electrons are the delimiting parameter for specific layers within the ionosphere.

The lowest layer of the ionosphere is the D-layer extending from 50 km to 90 km above the Earths surface. These altitudes vary some with season and magnetic latitude. The D-layer is characterized by highly complex chemistry due to it being

the boundary between the ionosphere and the neutral atmosphere below. This layer is responsible for the absorption of Lyman-alpha radiation and hard x-ray energy photons. Typical maximum values of electrons are on the order of 10^9 m^{-3} during the daytime. Due to the need of higher energy photons interacting in this layer, it essentially disappears during the local nighttime hours (Pisacane, 2008).

The next layer above the D-layer is the E-layer extending from 90-150 km. The E-layer is responsible for predominantly our protection from soft x-ray and some ultraviolet wavelength photons from the sun. The maximum concentration of electrons typically occurs around 120 km with values on the order of 10^{11} m^{-3}. Again, similar to the D-layer, due to the primary mechanism of electron-ion dissociation being solar input, the E-layer nearly disappears during the local nighttime hours (Pisacane, 2008). E-Layer electron densities decrease in the night by an order of magnitude due to recombination of electrons and ions and the lack of photons for continued ionization (Rishbeth and Garriott, 1969).

The upper most layer of the ionosphere is the F-Layer that extends from 150 km up to about 1000 km. The F-layer is the most stable layer of the ionosphere with less diurnal variation in overall electron concentration values. This layer absorbs extreme ultraviolet radiation through photoionization and during the day has two typical peak concentration values. The lower in altitude value is between $2\text{-}5\times10^{11}$ m^{-3} at a height of 180 km called the F1 peak. The upper maximum and overall greatest concentration in the ionosphere is the F2 peak with densities on the order 10^{12} m^{-3}. During the local nighttime, F1 densities can decrease up to an order of magnitude leaving only the F2 peak (Pisacane, 2008).

From Figure 1 the relative altitude extent of the D and E-layers can easily be contrasted with the extent of the F-Layer. While Figure 1 is the idealized state, there are many types of disturbances that can cause drastic changes to this picture

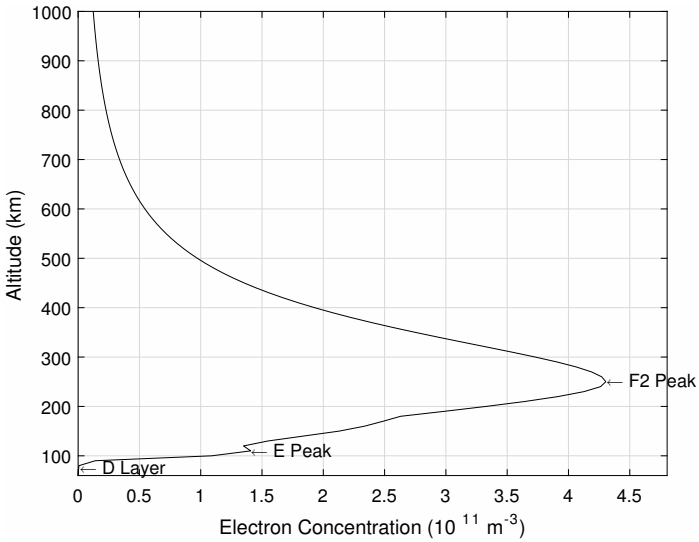

Figure 1. The structure of the Ionosphere in a normal or idealized state during solar minimum in the northern hemisphere mid-latitude summer at local noon. Graphic created using data from the International Reference Ionosphere model.

and will be discussed in the coming pages. Electron concentrations are also difficult to measure directly and generally don't tell us how the ionosphere is impacting our signals intended to pass through or reflect off certain layers. Specific measurement criteria and important values for this study will be covered in the next section.

2.2 Ionospheric Measurement Parameters

Now, with an understanding of the three basic layers within the ionosphere it's important to define the criteria used in describing this part of the atmosphere. As previously mentioned, heights of the maximum values are an imperative data point for understanding the current state. Due to the difficulty of direct measurement of electron concentrations, the critical frequencies of the layers are the baseline for describing the current state of the ionosphere.

In a uniform homogeneous plasma, this critical frequency is related to the electron density. As an electron is displaced from some equilibrium position a charge separa-

tion develops producing an electric field and a restoring force to attempt to maintain equilibrium. Due to the movement of the electron, it has inertia and therefore exhibits the motion of a harmonic oscillator (Gurnett and Bhattacharjee, 2005) with angular frequency

$$\omega_{pe}\,[rad/s] = \sqrt{\frac{n_e e^2}{m_e \epsilon_0}} \tag{1}$$

where n_e is electron density (m^{-3}), e is the charge of an electron (C), m_e is the electron mass (kg), and ϵ_0 is the permeability of free space ($C^2s^4m^{-4}kg^{-2}$). This plasma frequency is directly proportional to the electron concentration discussed in Section 2.1, and can be converted to MHz by

$$f_{pe}\,[MHz] = \frac{\omega_{pe}}{2\pi} \times 10^6 \tag{2}$$

The maximum values of electron concentrations for the D, E and F-layers of the ionosphere correspond to the critical frequencies. Critical frequencies are the maximum frequency that can be reflected by a medium (Schunk and Nagy, 2009). The frequency of the plasma becomes integral to the index of refraction described by

$$n = \sqrt{1 - \frac{\omega_{pe}^2}{\omega^2}} \tag{3}$$

where ω_{pe} is the plasma frequency described in Equation 1 (rad/s) and ω is the frequency of the signal (rad/s). Equation 3 demonstrates the critical frequency of a plasma showing that if $\omega < \omega_{pe}$, then the index of refraction is imaginary and an evanescent wave is produced.

For the purpose of this study, the focus is on the E-layer with foE as the critical plasma frequency of the E-layer being. A disturbance in the E-layer known as sporadic-E leads to another critical plasma frequency, foEs. Sporadic-E can be

more specifically defined as a blanketing event, fbEs, which is determined from the minimum frequency at which the ordinary wave reflections of the first order are observed from a layer at greater heights (Piggott and Rawer, 1978). A more detailed explanation of sporadic-E will be outlined in the next section. The corresponding heights associated with the foE and foEs are denoted with hmE and h′Es (Piggott and Rawer, 1978). To compare the Digisonde height measurements to the GPS-RO measurements, h′Es must be converted to an actual height. Figure 2 demonstrates these locations for the idealized ionosphere described in Figure 1. These factors help define the altitude and strength of the E-layer is, and if it is in a normal state or if there is a potential disturbance.

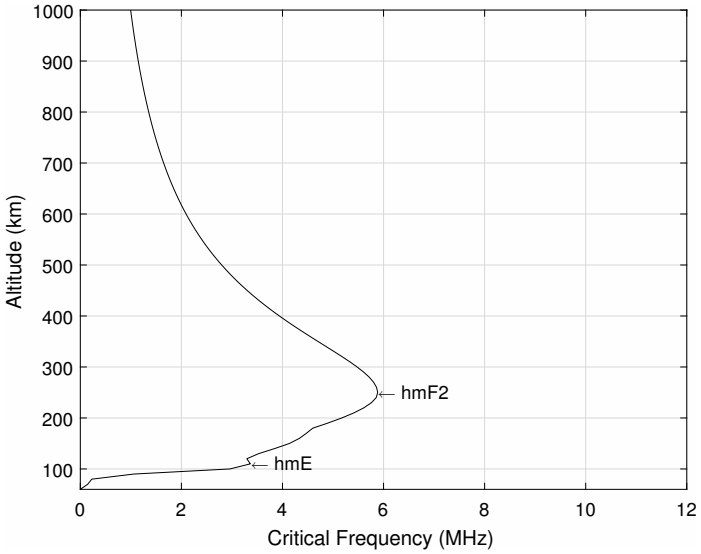

Figure 2. The structure of the Ionosphere in a normal or idealized state in frequency space during solar minimum in the northern hemisphere mid-latitude summer at local noon. Graphic created using data from the International Reference Ionosphere model.

2.4 Sporadic-E

There can be disturbances to the baseline or ideal ionospheric layers, the most prominent in the E-layer is known as sporadic-E. Sporadic is the term describing

these events because they don't occur in any particular pattern and they describe any abnormal reflection off of the E-layer (Piggott and Rawer, 1978). For this study, the focus will be on the enhancement in the electron density of the E-layer between approximately 90-120 km (Schunk and Nagy, 2009). These enhanced layers can occur at any latitude but are very prominent in the mid-latitudes. Electron densities can be increased up to an order of magnitude from the normal background.

The primary ions in this layer that help lead to the creation of the higher densities are metallic, Fe+, Mg+. Neutrals Fe and Mg are deposited through meteor ablation and ionized through the photoionization process. These metallic atoms have much lower ionization potentials and slower recombination rates than the typical constituents in this layer, O_2 and N_2. The dissociative recombination rates of O_2 and N_2 are approximately 2.4×10^{-7} (cm^3s^{-1}) and 2.2×10^{-7} (cm^3s^{-1}), respectively (Schunk and Nagy, 2009). The dissociate recombination rates of Fe+ and Mg+ are approximately 1×10^{-12} (cm^3s^{-1}) and 1×10^{-12} (cm^3s^{-1}), respectively (Bates and Dalgarno, 1962). This 5 order of magnitude difference in recombination rate leads to the long lived nature of the heavy metallic ions in the E-layer of Ionosphere.

The mechanism for creation of these thin layers is the $\vec{u_n}$ x $\vec{B}$ force, with $\vec{u_n}$ being the neutral wind velocity and $\vec{B}$ the magnetic field (Schunk and Nagy, 2009). A vertical wind shear will cause the $\vec{u_n}$ x $\vec{B}$ below the sporadic-E layer to push ions up the $\vec{B}$ field lines while opposite direction wind above the layer will cause downward vertical drifts leading to ion convergence. This ion convergence results in higher densities which lead to an increase in the critical frequency of the E-Layer (Schunk and Nagy, 2009).

The vertical ion velocity, w_z, required for E_s formation follows the simple model

$$w_z = \frac{1}{1+\gamma^2}\left(V\cos I\sin I + \gamma U\cos I\right) \tag{4}$$

where I is the magnetic inclination, γ is the ratio of ion-neutral collision frequency to the ion gyrofrequency, U is the zonal wind velocity, and V is the meridional wind velocity (Hines, 1964; Mathews, 1998; Whitehead, 1961). Below ~115 km, $\gamma \gg 1$ so the first term can be ignored. Sporadic-E layers are formed when zonal wind shear ($\partial U/\partial z < 0$ in the Northern Hemisphere) causes negative vertical ion convergence ($\partial w_z/\partial z < 0$).

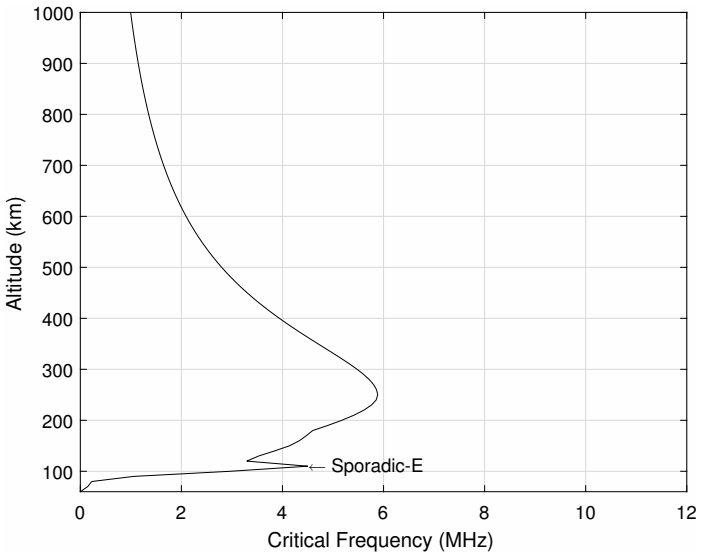

Figure 3. The structure of the Ionosphere with a sporadic-E layer present. Graphic created using data from the International Reference Ionosphere model with some manipulation.

Figure 3 demonstrates the how a sporadic-E layer leads to an abnormally high plasma frequency. The sporadic-E layers are typically thin vertically with thicknesses between 0.6-2 km and can sometimes present as multiple thin layers throughout the E-region (Schunk and Nagy, 2009). Horizontal extents of sporadic-E layers have been demonstrated through measurement by incoherent scatter radars to be between 10-1000 km with the average horizontal extent of a sporadic-E event of approximately 170 km (Whitehead, 1989). Sporadic-E clouds are not static in the atmosphere, they have horizontal motions of 20-130 m s^{-1} with drifts more eastward than the E-region

movement (Whitehead, 1989) and they can be present for minutes up to hours (Arras, 2010).

Some seasonal dependence has been shown for sporadic-E occurrence with Arras et al. (2008); Hocke et al. (2001); Wu et al. (2005) demonstrating that there is a maximum in occurrence in the summer hemisphere between 25-45° latitudes. There are also low occurrence rates around the magnetic equator due to the lack of vertical component of the magnetic field (Arras et al., 2008). So far there have been no conclusive studies linking sporadic-E occurrence to solar cycle dependence (Baggaley, 1984; Maksyutin et al., 2001), Maksyutin et al. (2001) demonstrated that there is a positive correlation between stronger sporadic-E layers and solar maximum due to the higher non-metallic ion concentrations.

This increase in critical frequency can have drastic impacts to communication signals attempting to pass through or reflect off the ionosphere. This study will primarily focus on the increases critical frequency of these sporadic-E layers due to their influence on radio signal propagation.

2.5 Ionosonde Measurement

Ionospheric measurement is predominantly performed through remote sensing techniques, i.e. not by instruments in the layer taking direct measurements. While each measurement technique has its upsides and downsides, this study utilizes the ionosonde measurement technique as the truth data. The ionosonde is a ground based antennae system that sends pulses vertically at specific frequencies intended to reflect off the ionosphere at an altitude where the signal frequency ω equals the plasma frequency ω_{pe}. The ionosonde sweeps a frequency range from about 1.6-12 MHz with a few gaps due to communication restrictions on those frequencies. The specific network of ionosondes utilized here is the Global Ionospheric Radio Observatory (GIRO)

Digisonde network maintained by Lowell Digisonde International.

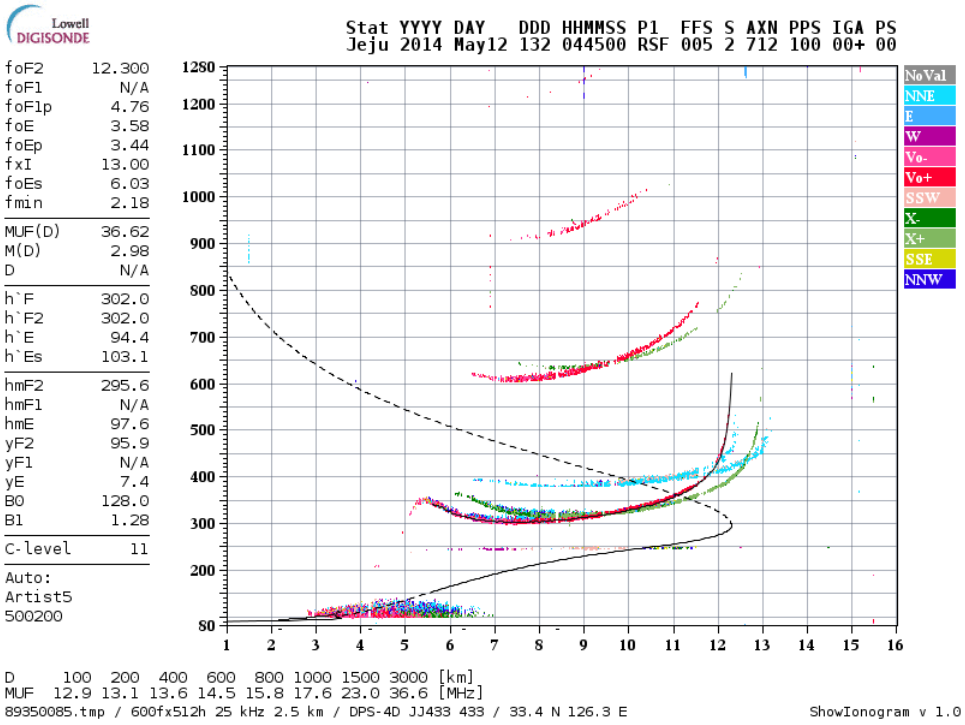

Figure 4. An Ionogram for Jeju Island, South Korea, Lat: 33.43 Long: 126.3, on 12 May 2014 with a sporadic-E event of fbEs of 5.60 MHz. (Center, 2018).

An example ionogram that is provided through the DIDBase for a sporadic-E event can be seen in Figure 4. Due to the blanketing sporadic-E event of 5.60 MHz, there is no information on the contents of the ionosphere from 103 km up to approximately 180 km because the layer prevents the signal from penetrating the E-region. This is a stark contrast to Figure 5.

This ionogram in Figure 5 has a lot more information about the lower Ionosphere because there isn't a blanketing sporadic-E event. This ionogram has only a data gap of approximately 20 km vs. the approximately 80 km for the sporadic-E event in Figure 4.

Figure 6 shows the current GIRO coverage, which has expanded from the coverage in the two years utilized for this study: 2010 and 2014. In 2010, there were 32

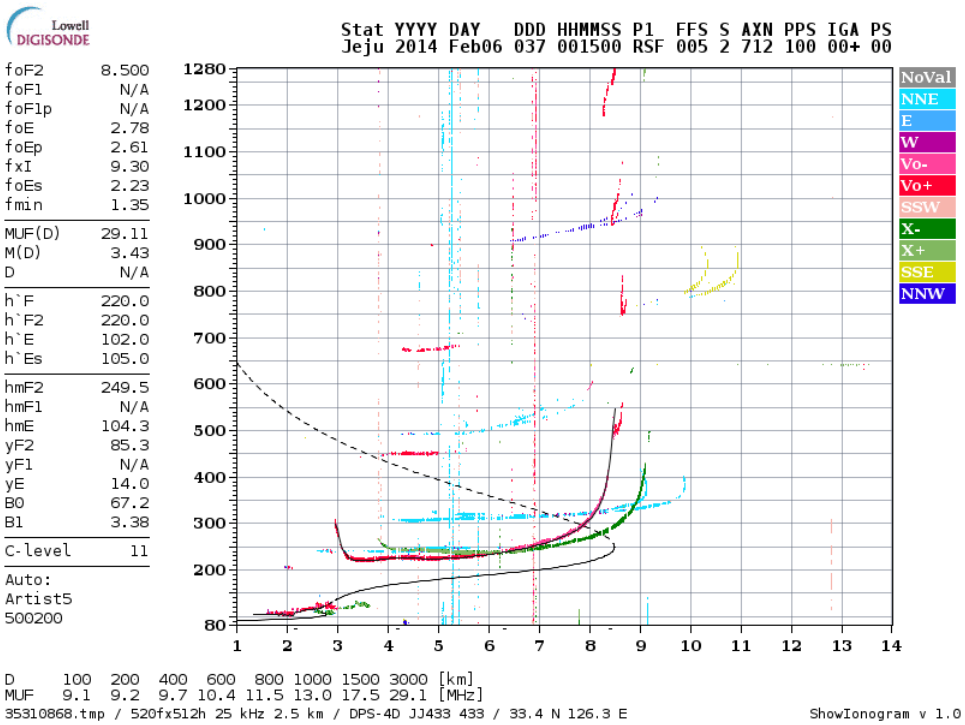

Figure 5. An Ionogram for Jeju Island, South Korea, Lat: 33.43 Long: 126.3, on 06 February 2014 without a sporadic-E event. (Center, 2018).

Digisondes as part of the GIRO network and by 2014 that was increased to 43 sites. This Digisonde network is able to provide real-time electron density profiles at each of the sites, with a sample rate of every 5 or 15 minutes. These measurements are stored within the Digital Ionogram Data Base (DIDBase), which allows for extraction of ionogram-derived characteristics such as the foEs and h′Es described in Section 2.3. For this study, the DIDBase characteristics are used as the baseline truth data for the identification of sporadic-E layers around the globe. Blanketing sporadic-E is more specifically defined as fbEs, which is determined from the minimum frequency at which the ordinary wave reflections of the first order are observed from a layer at greater heights (Piggott and Rawer, 1978). This was the baseline parameter for this study due to the fbEs corresponding to the maximum electron density in the layer (Arras, 2010).

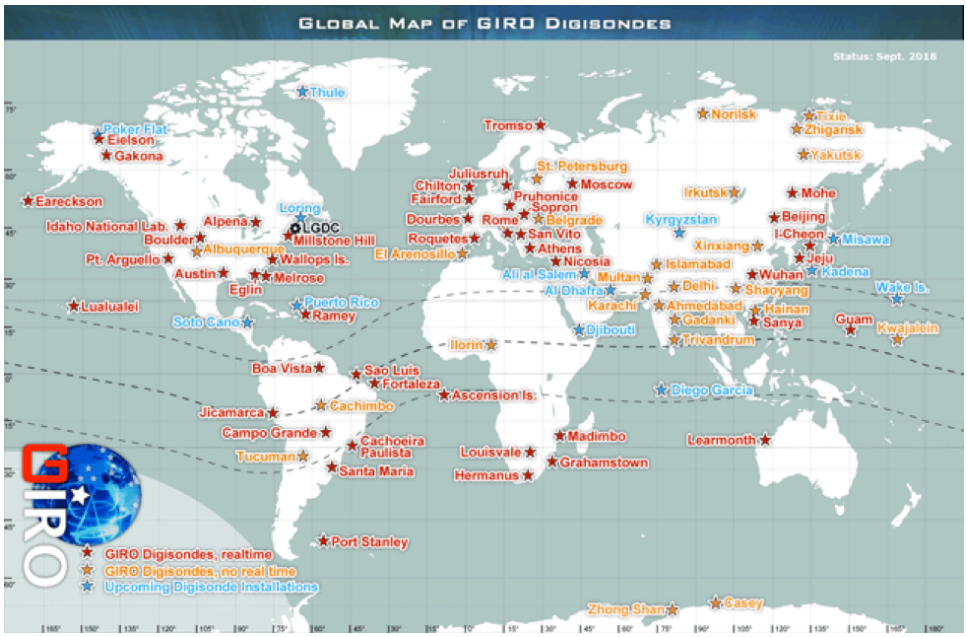

Figure 6. The global coverage of the GIRO Digisonde network as of September 2018 (Center, 2018).

While GIRO provides global coverage, there are still many areas of the world that can't be sampled due to the inability to put physical systems in place. Also, Figure 6 shows that there is good coverage in higher population density areas, but not in some potentially volatile military applicable areas, such the Horn of Africa and the Middle East. Expanding ionospheric sampling areas can provide a more comprehensive understanding of the current ionospheric state and provide real-time data to models and forecasts. The proper application of GPS-RO measurement discussed below can expand our global picture.

2.6 GPS Radio Occultation

GPS radio occultation is a remote sensing technique that analyzes GPS signals measured by low earth orbit (LEO) satellites to determine the conditions along the path. This study focuses on the use of the COSMIC LEO satellites. The GPS

satellite constellation consists of 24 GPS satellites orbiting Earth at about 20,200 km above the Earth's surface performing approximately two orbits per day (Schriener et al., 1999). The COSMIC constellation consists of six satellites at an altitude of about 800 km and orbital periods of 100 minutes, resulting in approximately 14 orbits per day (Arras et al., 2008). There are approximately 2,200 GPS radio occultation crossings daily, predominantly in the low to mid-latitudes (Arras et al., 2008). The GPS signals measured by COSMIC are the L1 and L2 frequencies, 1.57541 GHz and 1.22760 GHz, respectively (Hocke et al., 2001). The use of dual frequencies allows the elimination of non-ionospheric contributions to phase, such as the neutral atmosphere path delay and the delays due to system clocks (Manucci et al., 1999).

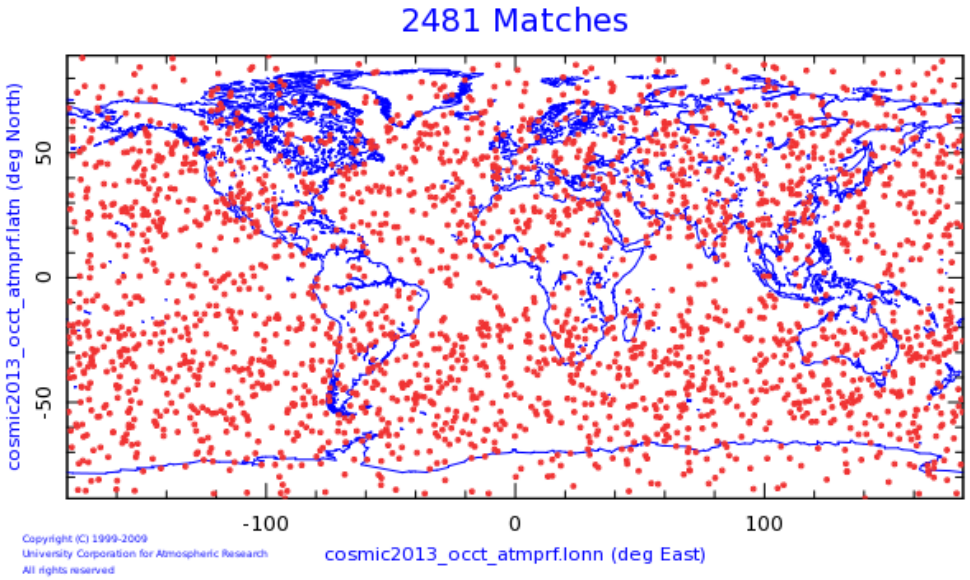

Figure 7. A map of GPS radio occultations for 29 Jun 2010. (UCAR, 2019)

Figure 7 shows the number and coverage of GPS radio occultations for 29 Jun

2010 with for 2,481 crossings globally. This large amount of occultations per day aid in the ability for global implementation for an observation technique. Arras (2010) shows that there are maximum globally at 25° N/S and 50° N/S due to the geometry between the LEO and GPS satellites for the E-region.

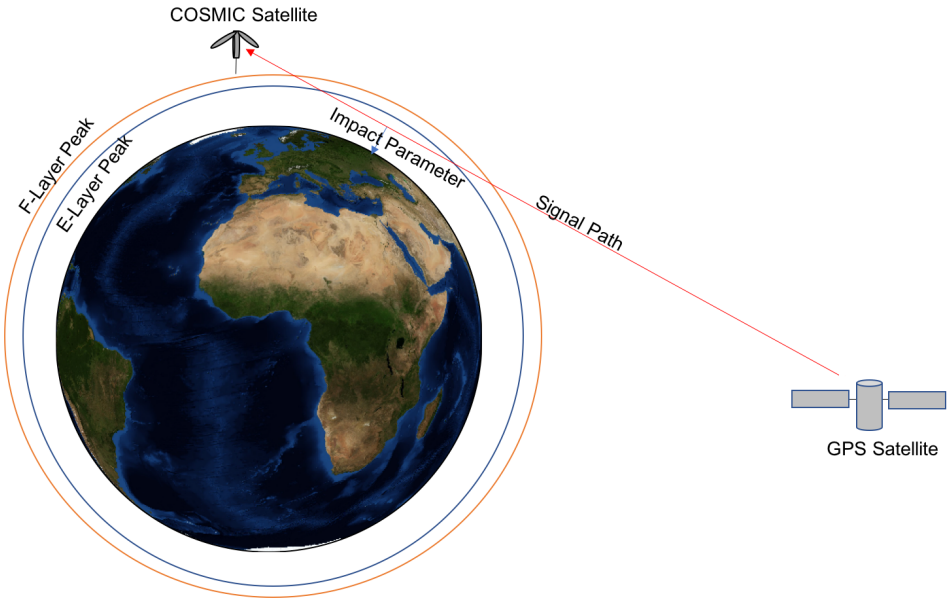

Figure 8. Illustration of the signal path between GPS and COSMIC satellites through the Ionosphere.

Figure 8 illustrates crudely the basics of the GPS to COSMIC signal propagation exploited in the radio occultation measurement technique. As the two signals transit the ionosphere, they are refracted by the change in the electron density of the signal path:

$$n \approx 1 - \frac{40.3 n_e}{f^2} \tag{5}$$

where n is the index of refraction, n_e is the electron density (m^{-3}) and f is the GPS signal frequency (Hz). The sharpest gradients in the ionosphere cause the most refraction to the two GPS signals. This refraction of the GPS signals is small enough to still assume a straight line propagation, with the worst case ionospheric conditions

only lead to bending of a few kilometers at most (Schriener et al., 1999). The GPS radio occultation data has a sample rate of 50 Hz which leads to the ability for it to detect small irregularities in the signal information (Arras et al., 2008). Additionally, the geometry of the LEO-GPS signal paths allows for an altitude slice of the ionosphere, which cannot be obtained using ground based GPS sensors. The combination of the high sample rate, the dependence on electron density, and the LEO-GPS geometry makes the GPS radio occultation technique ideal for measuring sporadic-E. From Figure 8, the assigned location for the GPS-RO crossing is the impact parameter, or the closest point of approach of the signal to the surface of the Earth.

There are two overarching ways to utilize this GPS radio occultation data in analysis of the E-layer of the ionosphere. The first approach is the use of the signal to noise ratio (SNR) and phase fluctuations to extract the contents of the signal path. The second approach to E-layer analysis is calculating the total electron content (TEC) using the excess phase difference on one of the signal frequencies. Hocke et al. (2001) did some of the initial work with the TEC method using the excess phase to calculate that TEC then using a sporadic-E cloud thickness of 0.6 km for the path length geometry. Pavelyev et al. (2003) utilized the radio holographic technique on the atmosphere and a reference climatological atmosphere and the difference yielded an electron density profile. Wu et al. (2005) used the signal to noise ratio to calculate variance of the F-layer, background E-layer, sporadic-E and total to calculate the sporadic-E event.

Arras et al. (2008) implemented a normalization of the SNR and the standard deviation of that normalized value was used to empirically categorize if there was a sporadic-E layer. Yakovlev et al. (2008) utilized fluctuations in amplitude and phase to locate sporadic-E layers with specific thresholds, characterized the layers into single, multiple or local plasma turbulence then calculated TEC. Zeng and Sokolovskiy

(2010) modeled tilted sporadic-E clouds to account for u-shaped structure in signal amplitude to account for varied thicknesses of the layers. Yeh et al. (2012) calculated the irregular degree index by normalizing the SNR, smoothing relative amplitude profile, decomposing the lower and upper envelopes then subtracting the lower from the upper and then removing the background.

Previous work by Chu et al. (2014) combined the SNR and TEC methods by implementing a high pass filter on the excess phase and SNR with constraints on the quality of the data for sporadic-E presence. Yue et al. (2015) used SNR to calculate S4 then set a threshold of greater than 0.3 for that value along with the obvious enhancement of TEC, and fluctuations in SNR and excess phase for identification of E_s layers. Niu et al. (2015) decomposed the TEC into high and low frequency wavelets and reconstructed the slant TEC to compare with the foEs values. Finally, Arras and Wickert (2018) normalized the SNR, calculated the S4 and empirically fit a comparison between the S4 value and the fbEs value.

As shown, the satellite based observation of the ionosphere using GPS-RO provides a unique data set of information for exploitation in many different ways. The GPS signals are distorted by gradients in the refractive index of the atmosphere, which can cause perturbations in the GPS phase (Hocke et al., 2001). The scintillation of the GPS signals is related to the magnitude of the electron density gradient and configuration of the satellites and sporadic-E layer (Wu et al., 2005; Zeng and Sokolovskiy, 2010). Additional information such as temperature, pressure, water vapor content and electron density profiles can be extracted from GPS-RO data.

Figure 9 shows the excess phase for both L1 and L2 signals provided by the GPS radio occultation data set from CDAAC. There is a clear disturbance in the phase just about the 100 km altitude in the phase information. This will be foundational to two of the techniques studied in this research project.

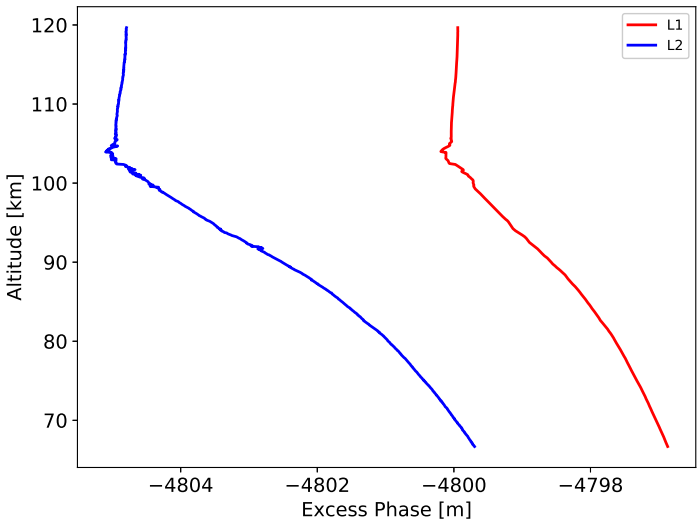

Figure 9. Excess phase provided by the GPS-RO data vs. altitude.

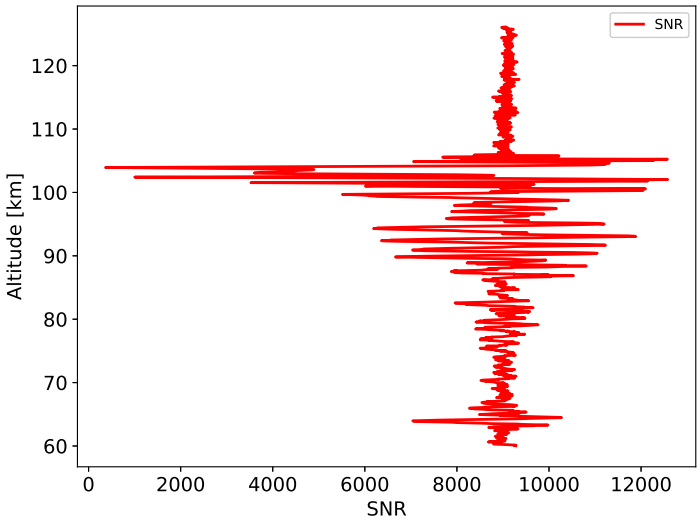

Figure 10. SNR for the L1 signal provided by the GPS-RO data vs. altitude.

Other information provided by the CDACC atmPhs files is the SNR of the L1 phase plotted in Figure 10. Both Figure 10 and Figure 9 are for the same cases and there is a very clear disturbance in the SNR just above the 100 km altitude. The SNR is foundational to two of the methods for exploitation of the GPS-RO data in this research endeavor.

III. Methodology and Results

The purpose of this chapter is to provide the development process for the data sets used throughout this experiment. It describes the four GPS-RO measurement techniques used in this comparison: an S4 calculation, TEC with a constant layer thickness, TEC with a variable layer thickness, and an Abel transform. The results of each method will accompany the description of each technique.

3.1 Data Set Development

This comparative analysis is derived from the GIRO network of Digisondes and the accompanying database of observations, DIDBase (International, 2019). The Digisonde locations with blanketing sporadic-E events (fbEs) is the ground truth of sporadic-E (E_s) intensity and height. GPS-RO crossings within 150 km and 30 minutes of these events were extracted from the COSMIC Data Analysis and Archive Center (CDAAC). This grid box is designed to capture the same events from the GPS radio occultation data that the ionosonde is observing. The average horizontal extent of a sporadic-E event is approximately 170km (Whitehead, 1989) with lifetimes of minutes up to hours (Arras, 2010).

3.1.1 Digisonde Data Base Extraction

The GIRO network comprised of Digisondes discussed in Chapter 2 provides the ground truth of E_s intensity and height. Specifically, the values of fbEs and h′Es, are extracted through the DIDbase on-line portal. Accompanying these values is an autoscaling confidence score, in a range of 0-100%, assigned by the DIDbase for confidence in the ionogram derived parameters. The fbEs value is the plasma frequency of the blanketing E_s layer. The h′Es value provided through the DIDBase is the

minimum virtual height of the E_s layer. The fbEs value corresponds to the maximum electron density in the profile which is the reason for its use in this study (Arras, 2010).

Some data set restrictions were developed through the DIDBase file acquisition process, and two years of data were processed through DIDBase, 2010 and 2014. Originally 2010 was meant to include a solar minimum year and 2014 a solar maximum for further comparison, but as the number of data points were refined this type of analysis was not feasible. This analysis focuses on low to mid-latitude sporadic-E, so only sites up to 55.47° for the Digisonde location near Moscow, Russia are included. In total there were 17 sites for 2010 and 26 sites for 2014 processed. The final discriminator on the Digisonde data set is the elimination of fbEs events with a low confidence score of below 10%.

3.1.2 GPS Radio Occultation Data Extraction

GPS radio occultation data extraction starts with utilizing the CDAAC web page (UCAR, 2019) to define an approximately 2° latitude by 2° longitude box around a Digisonde location. This is not an exact process due to restrictions on the latitude and longitude values having to be whole numbers. For example, for the aforementioned location of Moscow, Russia, with a latitude of 55.47° would have a window of 53° and 58°. This expansion allowed for all GPS-RO crossings within the 150 km box to be captured. The files retrieved from the CDAAC web page were the atmospheric excess phase file for use in the S4 calculation as well as the two TEC calculations. These files are abbreviated as atmPhs on the CDAAC website and are in netCDF format. The sample rate for the atmPhs files is 50 Hz or a resolution of approximately .05 km. The atmPhs files contain time dependent LEO and GPS positions along with SNR data for both L1 and L2 signals, and the excess phase for both signals. The

vertical extent of the atmPhs files corresponds to approximately 60 km to 140 km above the surface of the Earth. For the Abel Transform, a different type of file is required to include measurements of the topside ionosphere or generally, above the 140 km the atmPhs files. These ionPrf files contain an ionospheric data profile for a single occultation in netCDF format. The ionPrf files have a lower sample rate of 1 Hz or a resolution of about 2.7 km.

The GPS-RO files were extracted for all the 17 sites for 2010 and 26 sites 2014. This equates to 4,426 crossings for the 2010 sites and 6,389 for the 2014 sites with a total of 10,815 potential data points for comparison to the Digisonde soundings. This averages to about 251 crossings per site per year within the desired window.

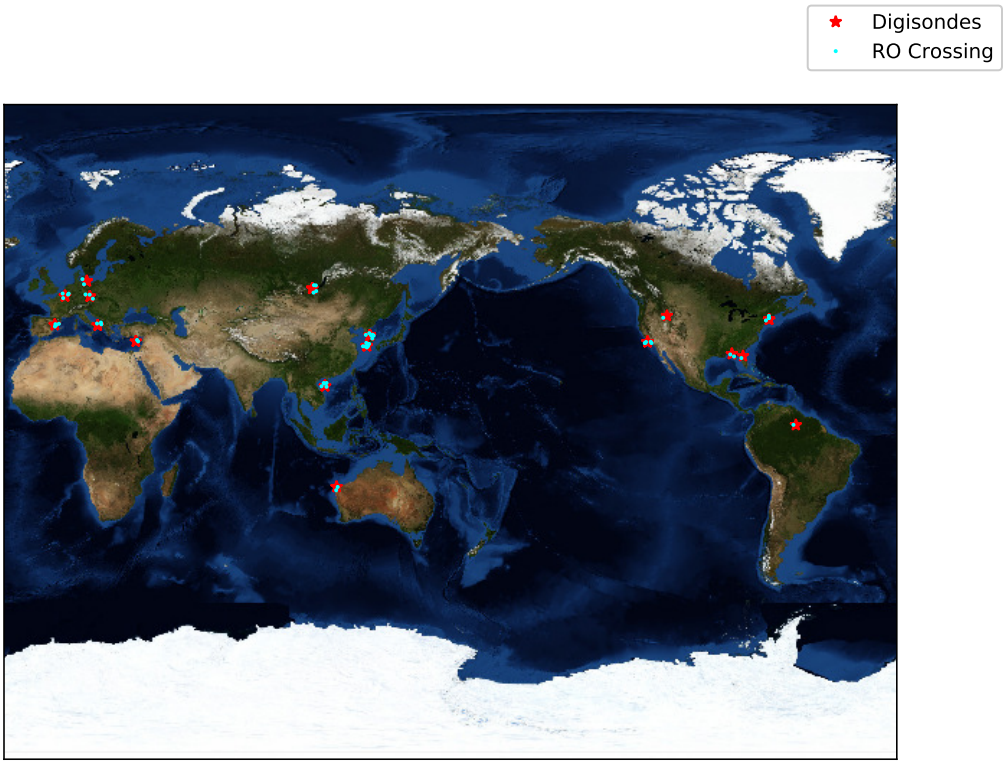

Figure 11. A global map of the Digisonde locations in the data set and the corresponding GPS-RO crossings.

Figure 11 shows the global distribution of the Digisonde locations and the GPS-RO crossings that corresponded to those locations. The map illustrates the existence of sporadic-E in mid and low latitudes as well as northern and southern hemispheres.

3.1.3 Digisonde to GPS Radio Occultation Data Matching

The first step in matching the Digisonde and GPS-RO data involves determining if sporadic-E was measured by the GPS-RO crossings. Three different binary requirements are placed on the GPS-RO data to ensure measurement of a sporadic-E layer. The first is the use of a rolling standard deviation of the L1 signal over a 2 km window equating to greater than 0.2, indicating there is sporadic-E along the signal path (Arras and Wickert, 2018). The second is the requirement for the phase perturbations of both the L1 and L2 signals to be greater than 5 cm indicating a large electron density gradient (Chu et al., 2014). The third requirement demands S4 values greater than 0.15 which will be further described in the next section (Arras and Wickert, 2018). If these three criteria are met for the GPS-RO data, these files are then compared to the locations and times of the Digisonde measured fbEs values.

To compare the time and locations of the GPS-RO measured sporadic-E with the Digisonde parameters, a position and time must be assigned to each RO crossing. To assign a position to the RO measurement for each point in time, the impact parameter is calculated over time neglecting the small bend in the signal at ionospheric altitudes (Schriener et al., 1999), and the point corresponding the impact parameter (closest point to Earth) is used as the position of measurement. For this assessment, the time given to the crossing location is the time assigned to the height of 100 km according to the RO data. The average sample length contained in the atmPhs files is less than two minutes. This ensures that with a sample rate of 5 or 15 minutes by the Digisonde, any time difference of less than 30 minutes shouldn't be missed. Due to

the constraint on the fbEs measurements from the Digisondes, some time window was needed for the matching of events.

For example, if a Digisonde registered an fbEs event with higher than 10% confidence score at 1030, but no other fbEs measurements within 30 minutes; as long at the GPS-RO crossing was between 1000-1100 and 150 km in horizontal extent, it would be recorded as a matching case. Due to the high sample rates of 5 or 15 minutes of the Digisonde, many of the GPS-RO times would relate to multiple fbEs readings, i.e. there are multiple fbEs recordings within 30 minutes of the GPS-RO crossing. To match the GPS-RO to just one Digisonde measurement, the closest time to the GPS-RO time was selected.

Through these data restrictions there were 140 matches across the two years. Though these cases met the necessary criteria laid out above, some additional conditions were enforced involving visual inspection of the data. One of the most prevalent disfigurations to the data is normalized SNR values that are highly erratic. The binary requirements placed on the GPS-RO data are met for this highly erratic SNR, but the large fluctuation in SNR is observed over all altitudes and not localized in a small region as expected for sporadic-E. Also, some of the excess phase data is not consistent with previous literature and leads to highly abnormal TEC calculations, so they are eliminated from the comparison. Because the TEC measurements use dual frequency data, if one of the excess phase slopes with respect to altitude don't closely follow one another, the calculated TEC values can become orders of magnitude too large.

So far, the discussion on data quality has been on the GPS-RO data. There were also inspections of all the ionograms from DIDBase to ensure that the Digisonde data points were trustworthy. After all case study restrictions were placed on the combined data sets between the Digisonde and GPS-RO files, a total of 65 case

studies emerged as quality data points. Overall, these cases are independent dates and times for the different locations. One day, 23 Aug 2014, registered three different Digisonde measurement times at one location, El Arenosillo, Spain with three separate GPS-RO crossings occurring within 30 minutes of those measurements, 1158Z, 1557Z and 2050Z. There are 20 cases in 2010 and 45 in 2014, again hindering the possible comparison of solar maximum and solar minimum with a limited data set.

3.2 Conversion of Virtual Height to Actual Height

Previous studies of sporadic-E using GPS radio occultation perform comparisons between the virtual height of the ionosonde and the height of the layer as determined by the sporadic-E measurement technique. In an effort to convert the virtual height to a true height, this study used ionogram derived electron density profiles from DIDBase to determine the actual height of the sporadic-E layer. Through a simple integration of the group index of refraction in Equation 7, from the base of the ionogram to the virtual height, using the frequency from each height and the fbEs value as the signal frequency, the actual height of the sporadic-E cloud can be estimated through

$$h' = \int_0^h n_g \, dh \tag{6}$$

$$n_g = \frac{1}{\sqrt{1 - \left(\frac{f_p(h)}{fbEs}\right)^2}} \tag{7}$$

where h is the actual height, h' is the virtual height, n_g is the group index of refraction, f_p is the plasma frequency as a function of altitude, and fbEs is the blanketing sporadic-E frequency (Rishbeth and Garriott, 1969). The Digisonde measurements provide plasma frequencies for altitudes above 90 km, so $h' = h$ if $h \leq 90$ km. Therefore, this integration is slightly incomplete due to the missing ionogram measurements

of the lowest portion of the ionosphere. The lower bound of the ionogram being only down to approximately 1.6 MHz means that the ionogram drawing software performs a best fit for the D-layer and the lower E-layer. For the purposes of this study, the corrected height of the fbEs using this method will be considered the truth height for ionogram measurements.

3.3 Frequency and Height Calculation Using S4

The first measurement technique applied to the 65 case studies uses the SNR to calculate the S4 as performed in Arras and Wickert (2018). S4 is the scintillation index or the normalized root-mean squared deviation of signal strength:

$$S_4 = \sqrt{\frac{(\langle SI^2 \rangle - \langle SI \rangle^2)}{(\langle SI \rangle^2)}} \tag{8}$$

where SI is the SNR provided by the GPS radio occultation data (Van Dierendonck and Arbesser-Rastburg, 2004). This method captures the location corresponding to the largest fluctuation (interference) of the signal as it passes through the ionosphere. For the purposes of this study, the L1 GPS signal is used due the higher frequency which is less noisy.

3.3.1 S4 Methods

The S4 technique in Arras and Wickert (2018) normalizes the SNR for the L1 GPS signal and calculated the standard deviation using a 2 km sliding window. Arras and Wickert (2018) includes only cases with an empirically determined standard deviation greater than 0.2 within a 10 km altitude. The S4 for these cases is calculated using 25 points above and below the peak in the standardized SNR. After the S4 is calculated,

a linear fit of the ionosonde measured fbEs to the GPS-RO is performed resulting in

$$fbEs\ [MHz] = 3.8 * S4 + 2.0 \tag{9}$$

A total of 17 points were used to determine this fit, with an R value of 0.79 indicating a good fit to the data. Implementation of the Arras and Wickert (2018) work is straightforward utilizing Equation 8 with the normalized SNR as the signal strength, and averaging calculated over a 2 km sliding window. An example of the S4 calculated from the GPS-RO data as a function of altitude is displayed in Figure 12. The peak S4 of approximately 0.30 is located slightly above 100 km.

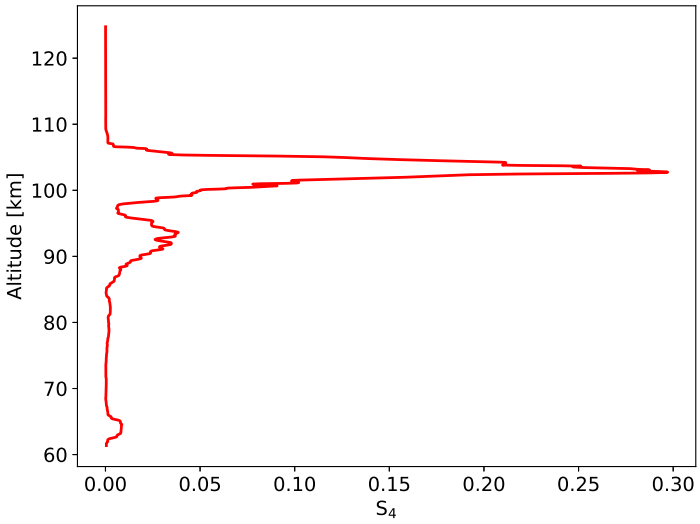

Figure 12. A sample of GPS-RO S4 calculations using the normalized L1 S4 as a function of altitude.

The next step in determining the critical frequency using the S4 involves locating the maximum S4 value and associated altitude. Figure 12 shows only one sharp peak in S4 near the 100 km altitude, but not all S4 calculation plots are as clearly defined in having a singular peak. For this reason, calculated heights of sporadic-E layers were limited to between 80-120 km which encompasses the varying altitude ranges

indicated throughout literature of observed occurrences. All calculations of the S4 method were performed through automated means with a human in the loop as a quality check at the end. After retrieving the maximum S4 and its associated height, the conversion to a usable critical frequency is performed using Equation 9.

3.3.2 S4 Results

The S4 calculated fbEs values are compared on a case by case basis with the appropriate Digisonde observations. Each comparison assumes that the Digisonde observations are the truth value and that a perfect S4 calculated fbEs value would exactly match. Figure 13 illustrates the effectiveness of the S4 method, and shows that this technique performs well for some of the 65 cases, but has large errors on other observations. The S4 calculated fbEs values are mainly grouped between 2.5 and 4 MHz while the Digisonde values are primarily grouped between 2 and 5 MHz.

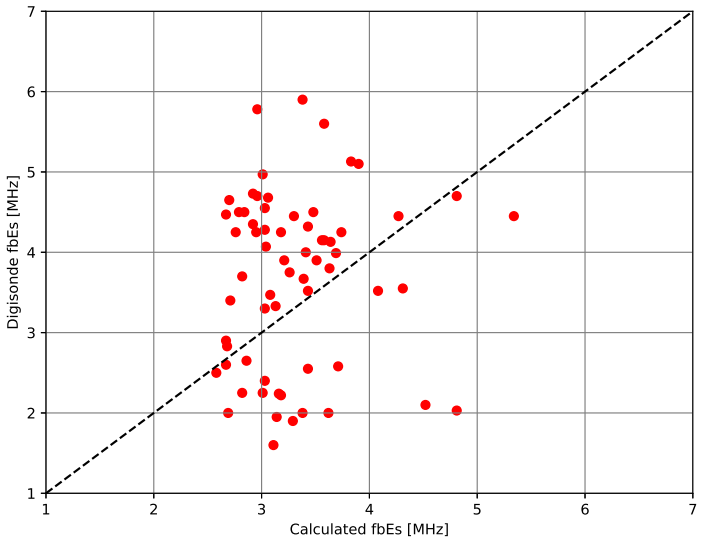

Figure 13. The calculated fbEs using the S4 method compared to the Digisonde fbEs observation, with the dashed line as a perfect relationship.

An error plot can help inform on the ability of the S4 method to accurately depict

the Digisonde measured value. Figure 14 shows the case by case error in the calculated fbEs and highlights some of the large discrepancies. The largest error recorded through this method was -2.82 MHz. Conversely, the most accurate calculated value had an error of only 0.07 MHz. Overall, the S4 method for calculating fbEs shows relatively large errors, with 30 data points with errors greater than 1 MHz.

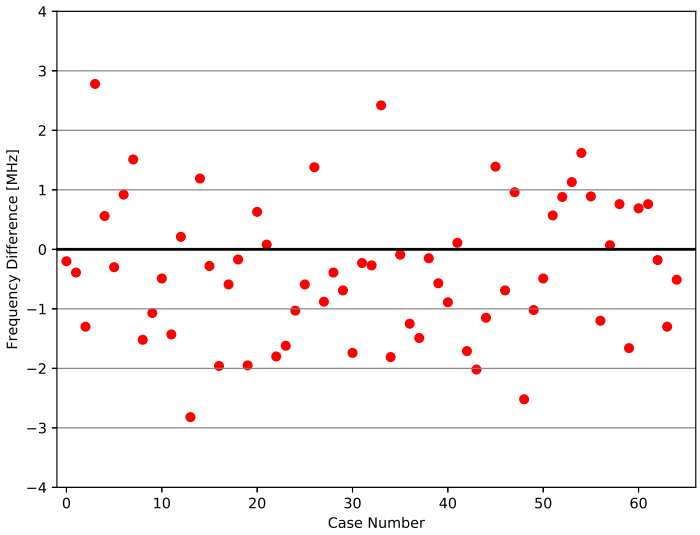

Figure 14. The difference between the observed Digisonde fbEs value and the calculated fbEs for each case using the S4 method.

Table 1. The average, standard deviation, root mean square error (RMSE), mean absolute error (MAE), relative mean absolute error (RMAE), and r^2 values for the comparison between the Digisonde fbEs values and the fbEs values for the S4 fbEs calculation technique. The error values are have units of MHz.

Method	Avg	Std Dev	RMSE	MAE	RMAE	r^2
S4	3.32	0.56	1.23	1.01	0.30	0.01
Digisonde	3.67	1.07	N/A	N/A	N/A	N/A

Table 1 shows the difference between the S4 fbEs calculation technique and the Digisonde data set statistically. Overall, the S4 technique underestimates the fbEs values with a much smaller spread in the data indicated by the smaller standard deviation. This is indicative of the inability of the S4 method to handle the largest

fbEs values as also shown in Figure 13 with all Digisonde values greater than 5 MHz being well underestimated by more than 1 MHz. The r^2 measure of correlation highlights the weakness of the S4 method with a value near zero indicating that the relationship is almost random. Due to the S4 calculation being built upon a linear fit between the S4 value and the fbEs, this low r^2 value undermines the strength of that relationship and suggests that a nonlinear relationship may exist.

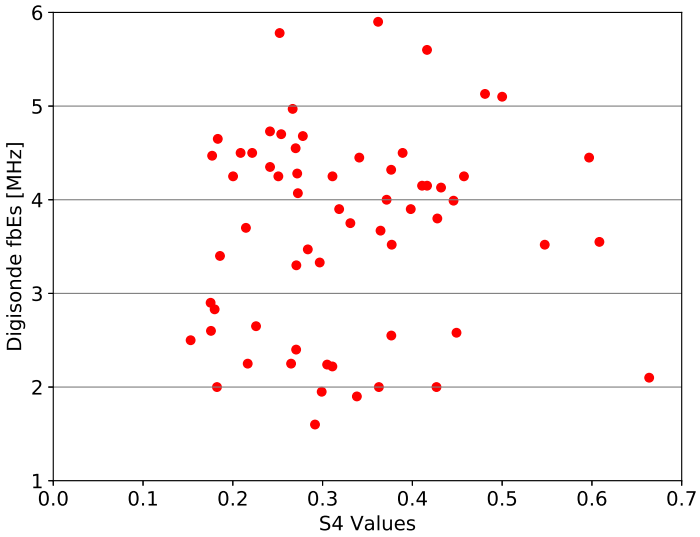

Figure 15. The S4 values calculated from the GPS-RO data compared to the fbEs values from the Digisondes.

As seen in Figure 15, it is apparent in this data set that there is not a linear relationship between the S4 values and the fbEs vales as postulated in Arras and Wickert (2018). The low r^2 value is well demonstrated in Figure 15.

The S4 calculated sporadic-E heights were also compared on a case by case basis with the calculated actual heights derived from Digisonde measurements. Each comparison encompasses an assumption that the calculated actual height are the truth value and that a perfect S4 altitude value would exactly match. Figure 16 illustrates the effectiveness of the S4 height measurements and shows a wider spread in predictions than for the intensity estimates. The majority of S4 estimated heights are

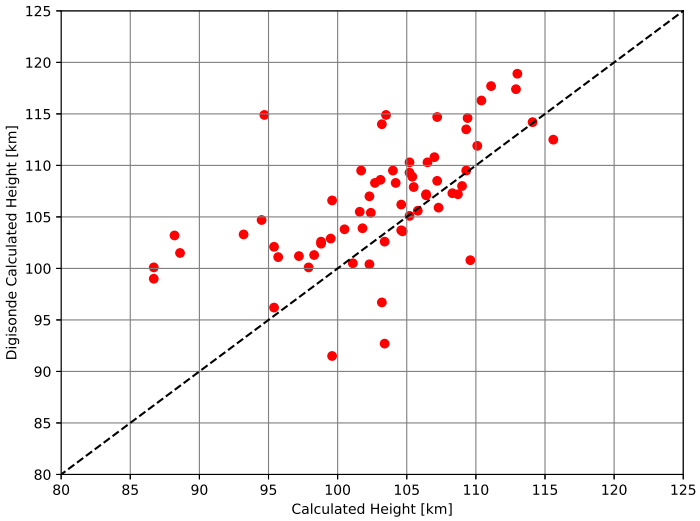

Figure 16. The calculated height using the S4 method compared to the Digisonde derived actual height, with the dashed line as a perfect relationship.

between 95 and 110 km, while the Digisonde heights are mainly between 100 and 115 km. Figure 17 shows the case by case error in the calculated heights and highlights some of the large discrepancies. The largest error recorded through this method is -20.2 km. Conversely, the most accurate calculated value has an error of only 0.1 km. Overall, this method shows a bias for underestimating the height of the fbEs layer in the ionosphere by 3.5 km.

Table 2. The average, standard deviation, root mean square error (RMSE), mean absolute error (MAE), relative mean absolute error (RMAE), and r^2 values for the comparison between the Digisonde calculated heights and the determined heights for S4 height calculation technique. The error values have units of km.

Method	Avg	Std Dev	RMSE	MAE	RMAE	r^2
S4	103.0	6.3	6.4	4.9	0.05	0.37
Digisonde	106.5	5.8	N/A	N/A	N/A	N/A

Table 2 highlights the difference between the S4 height calculation and the Digisonde derived actual height data set. The S4 method consistently underestimates the height of the sporadic-E layer and shows a slightly larger spread than the Digisonde heights. This method is most accurate near the average height of the Digisonde (107 km)

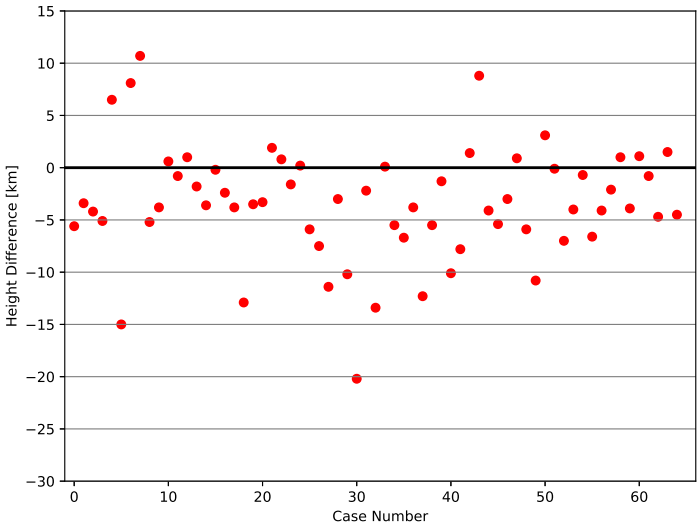

Figure 17. The difference between the Digisonde derived actual heights and the calculated height for each case using the S4 method.

as shown in Figure 16 with many of the largest errors occurring on the lower and higher Digisonde measured heights. The r^2 value shows that the heights are highly correlated, which is also shown by a majority of the differences in Figure 17 being less than 5 km. More analysis of the effectiveness of the S4 method is provided in the comparison between each method at the end of this chapter.

3.4 Frequency and Height Calculation Using TEC with Constant Thickness

The second measurement technique applied to the 65 case studies uses the excess phase to calculate relative TEC values and assumes a constant sporadic-E thickness to convert the TEC to an electron density. This electron density is then converted to a plasma frequency using Equation 2. The relative TEC values are calculated through use of the excess phase from both the L1 and L2 GPS signals. This method is based on work by Hocke et al. (2001), and requires more effort than the simple S4 technique.

3.4.1 TEC with Constant Thickness Methods

The frequency and height calculations using relative slant TEC with constant thickness begins with the calculation of the TEC profile. The method applied in this study utilizes the dual frequency TEC calculation outlined in Hocke et al. (2001) as

$$TEC\,[e^{-}/m^{2}] = \frac{1}{40.3}\left(\frac{f_1^2 f_2^2}{f_1^2 - f_2^2}\right)(S_1 - S_2) \tag{10}$$

where, $f_1 = 1.57541$ GHz is the L1 GPS frequency, $f_2 = 1.22760$ GHz is the L2 frequency, S_1 is the excess phase of L1 in m, and S_2 is the excess phase of L2. The relative slant TEC must be detrended to obtain the perturbations in TEC due to the sporadic-E layer. The relative TEC profile is filtered with a low pass filter over a 7 km moving average. The difference of the raw TEC and filtered TEC provides fluctuation on the scale smaller than 7 km. These fluctuations are then converted to an electron density by dividing by an effective path length across the sporadic-E layer:

$$\Delta n_e \sim \frac{TEC - \langle TEC \rangle}{2\sqrt{2R\Delta R}} \tag{11}$$

where n_e is the electron density, TEC is the raw TEC, $\langle TEC \rangle$ is the filtered TEC, R is the radial distance from the center of Earth to the layer in meters and ΔR is the thickness of the sporadic-E layer in meters (Hocke et al., 2001). Due to TEC being the line integration of the electron density, the TEC requires a third dimension for the estimation of the electron density. This geometry is assumed to be a cylinder centered around the tangent point with an effective horizontal tube length of $2\sqrt{2R\Delta R}$ (Ahmad, 1998). The denominator in Equation 11 is the effective path length through the sporadic-E layer using this geometry, with the R≈6470 km and the layer thickness ΔR assumed to be 0.6 km. For this constant thickness method, the thickness is held constant for all calculations at a value of approximately 180 km. This length agrees

with early estimations of the horizontal extent of sporadic-E in the range of 10-1000 km with an average of 170 km (Whitehead, 1989).

Execution of the theory from Hocke et al. (2001) is not as simple as the Arras and Wickert (2018) implementation. The first step in the process requires the excess phase data from the atmPhs files to calculate a relative TEC. Because the TEC is relative and not absolute, the departure from some baseline TEC is needed for analyze the contribution from a sporadic-E cloud, referred to as the detrended TEC value. The baseline TEC will be referred to as the filtered TEC and is smoothed over a 30 km moving average using the Savitzky-Golay fit technique to a 3rd degree polynomial (Chu et al., 2014). This filtered TEC is then subtracted from the unfiltered relative TEC to find the largest deviation, which is assumed to correspond to the highest electron density concentration in the sporadic-E layer. To reduce noise in the detrended TEC, a Savitzky-Golay filter with a 1 km moving average is applied. It must be noted that different methods of detrending cause slight differences in the results. The 30 km average was determined through attempting to capture the long term changes and eliminating the small fluctuations. The 1 km average was determined through trial and error at finding a method for capturing the small variations without too much noise in the data.

The largest difference provides indication for the value of the TEC at the sporadic-E layer, though this allows for the magnitude of the filtered TEC in the layer to have influence in that difference calculation. In an attempt to find the base of the layer and remove that influence of that from the calculated electron density, the first zero point of the detrended TEC below the peak layer is used as the base. The magnitude of the TEC for the layer is then selected as the difference between relative TEC at the altitude corresponding to the peak in the detrended TEC and the relative TEC at the altitude of the base.

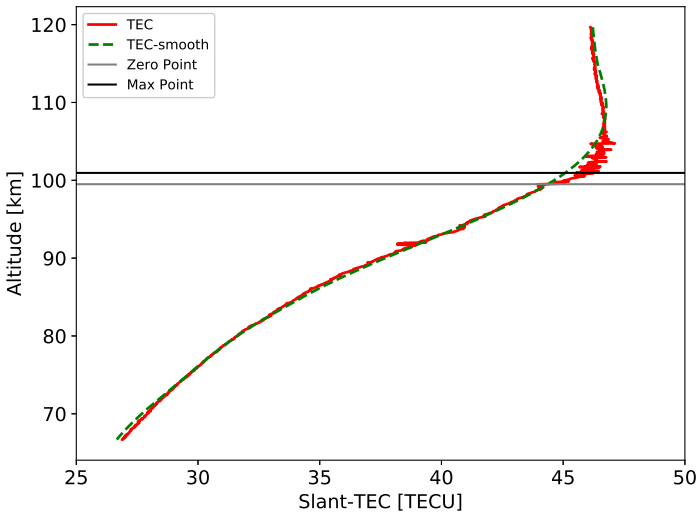

Figure 18. Both the relative and TEC and filtered TEC vs. altitude using the TEC method

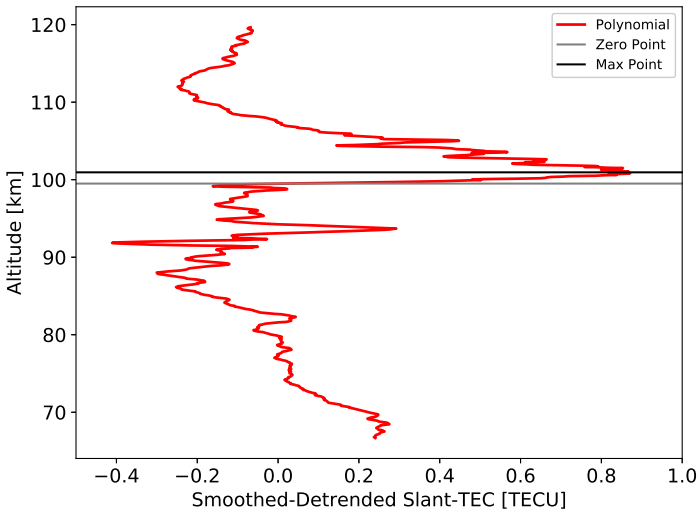

Figure 19. The difference between the relative TEC and filtered TEC vs. altitude using the TEC method

Figure 18 illustrates the relationship between the relative TEC and the filtered TEC. The differences between the relative and filtered (smooth) TEC can still be very small even though they are smoothed over much different scales. The aim is to capture the true perturbation in the signal by the strong gradient of the sporadic-

E layer. This difference should be the greatest in the noisy area around 100 km. Figure 19 shows the difference between those two values with an obvious peak to the detrended value near 100 km. Without the correction of finding the bottom of the sporadic-E layer, the detrended value would be the numerator of Equation 11. However, this technique consistently underestimated the TEC magnitudes for the sporadic-E layers, and the use of a difference between the relative TEC for the base and peak detrended altitudes provides more realistic TEC values. The horizontal lines on both Figure 18 and Figure 19 illustrate for this case where the zero point is and the maximum of the detrended. The peak in Figure 19 is assigned as the height as calculated by the TEC methods.

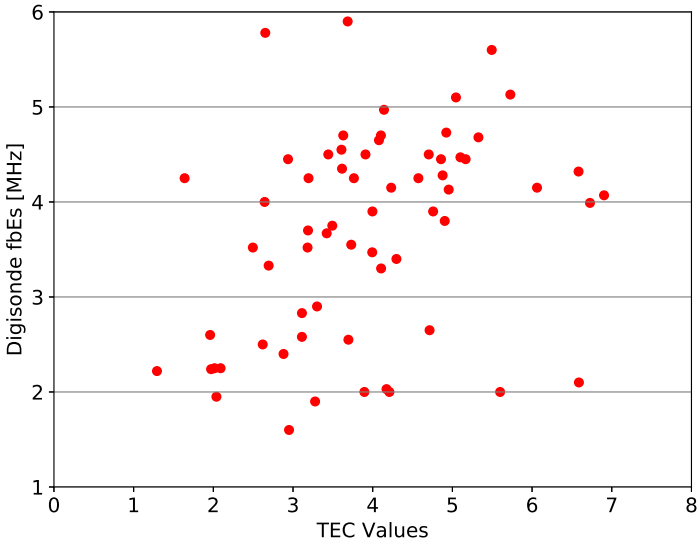

Figure 20. The Digisonde fbEs values compared to the detrended TEC values used for the electron density calculations.

Figure 20 shows the relationship between the Digisonde fbEs readings and the detrended TEC values calculated through this study. The relationship of the values is much stronger than the S4 to fbEs in Figure 15.

3.4.2 TEC with Constant Thickness Results

The TEC with constant thickness calculated fbEs values are compared on a case by case basis with the appropriate Digisonde observations. Each comparison encompasses an assumption that the Digisonde observations are the truth value and that a perfect TEC with constant thickness calculated fbEs value would exactly match. Figure 21 show the results of the intensity estimates using the TEC with constant thickness method. This technique performs well for a fair amount of the 65 cases and follows the general shape desired, but has large errors on some observations.

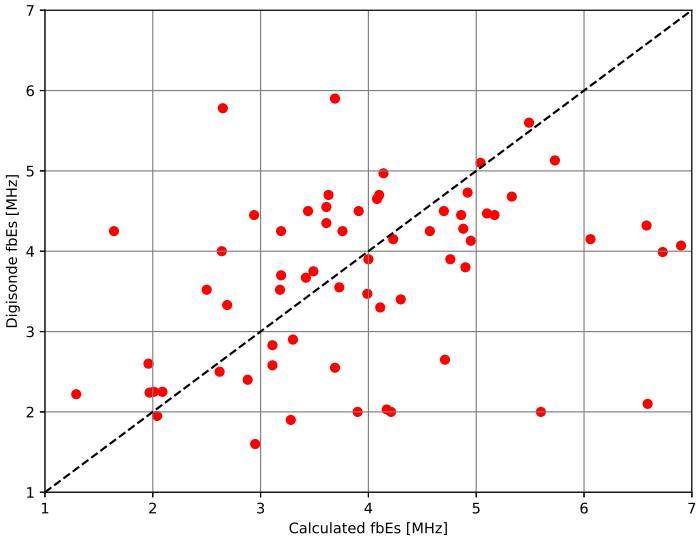

Figure 21. The TEC with constant thickness calculated fbEs compared to the Digisonde fbEs observation, with the dashed line as a perfect relationship.

Figure 22 shows the case by case error in the calculated fbEs values and highlights some of the large discrepancies. The largest error recorded through this method is 4.49 MHz. Conversely, the most accurate calculated value has an error of only -0.06 MHz. Overall, the TEC with constant thickness method for calculating fbEs shows relatively large errors. There are 21 data points with larger than 1 MHz of error, and 3 points with absolute errors greater than 3 MHz.

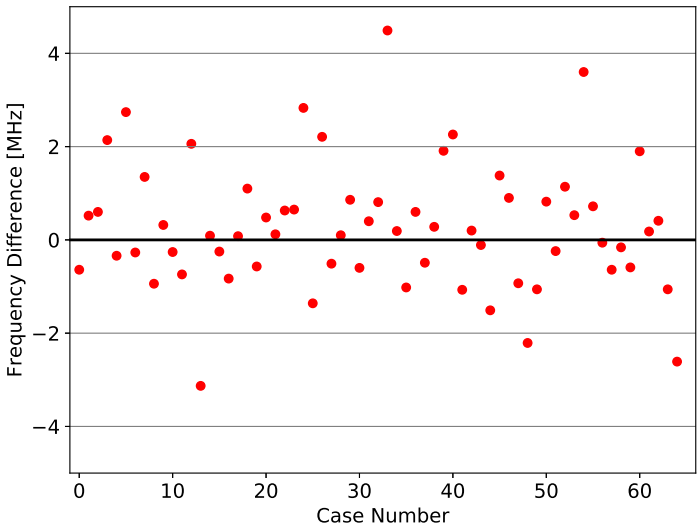

Figure 22. The difference between the observed Digisonde fbEs value and the calculated fbEs for each case using the TEC with constant thickness method.

Table 3. The average, standard deviation, root mean square error (RMSE), mean absolute error (MAE), relative mean absolute error (RMAE), and r^2 values for the comparison between the Digisonde fbEs values and the fbEs values for the TEC with constant thickness fbEs calculation technique. The error values have units of MHz.

Method	Avg	Std Dev	RMSE	MAE	RMAE	r^2
TEC w/ con ΔR	3.94	1.27	1.38	1.01	0.33	0.118
Digisonde	3.67	1.07	N/A	N/A	N/A	N/A

Table 3 highlights the statistical relationship between the TEC with constant thickness calculated and the measured Digisonde fbEs values. This method slightly overestimates the fbEs values by 0.3 MHz on average. This is likely indicative of the variability in the true thickness of the sporadic-E layers and that they aren't all 0.6 km. It also shows that there is a large spread in the values, 0.2 MHz larger than the Digisonde fbEs measurements. The value of r^2 shows that there is a medium strength correlation between the calculated and Digisonde fbEs, but not a strong one.

The TEC calculated sporadic-E layer heights are also compared on a case by case basis with the appropriate Digisonde derived actual height. Each comparison encompasses an assumption that the calculated actual height are the truth value and

that a perfect TEC altitude value would exactly match. The results are displayed in Figure 23 showing that the GPS-RO measurements underestimate the heights on average.

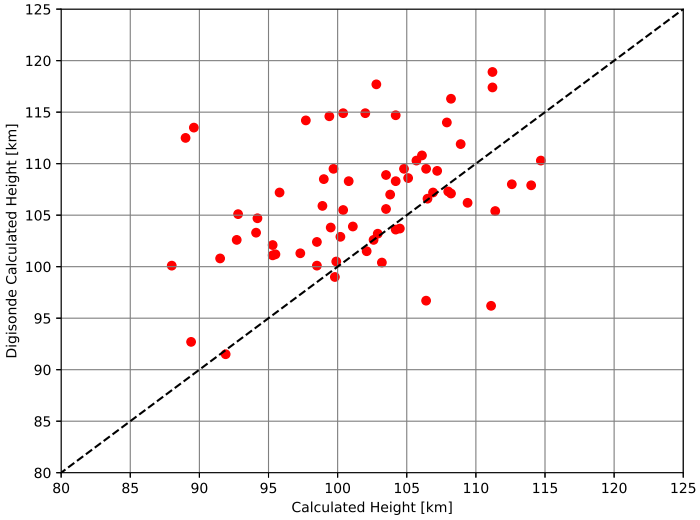

Figure 23. The TEC method calculated height compared to the Digisonde calculated height with the dashed line as a perfect relationship.

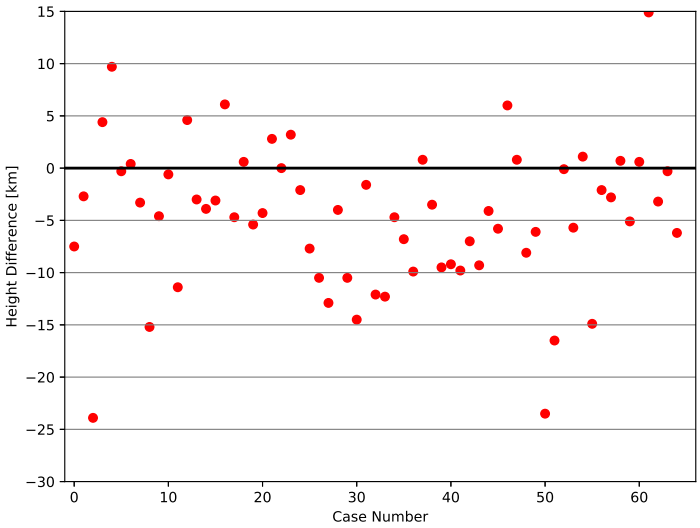

Figure 24. The difference between the calculated Digisonde height and the TEC calculated height for each case.

Figure 24 shows the case by case error in the heights and highlights some of the

large discrepancies. The largest error recorded through this method is -23.9 km, and the most accurate value is zero to the number of significant digits in the height calculation. Overall, there is a bias for underestimating the height of the sporadic-E layer, similar to the results from the S4 technique.

Table 4. The average, standard deviation, root mean square error (RMSE), mean absolute error (MAE), relative mean absolute error (RMAE), and r^2 values for the comparison between the Digisonde calculated heights and the determined heights using the TEC height calculation technique. The error values have units of km.

Method	Avg	Std Dev	RMSE	MAE	RMAE	r^2
TEC	101.9	6.4	8.3	6.4	0.06	0.14
Digisonde	106.5	5.8	N/A	N/A	N/A	N/A

Table 4 highlights what is shown in Figure 23 and Figure 24 that the TEC method for height measurement consistently underestimates the sporadic-E layer height by 4.6 km on average. The TEC method has a slightly larger spread than the Digisonde heights by 0.6 km. A medium strength correlation is observed for the two data sets. More analysis on the effectiveness of the TEC with constant thickness method is provided at the end of this chapter.

3.5 Frequency Calculation Using TEC with variable thickness

The implementation of the frequency calculation through TEC with variable thickness was designed to better capture the physical nature of the sporadic-E layer. In Section 3.4, the constant thickness is not physically realistic, because not every sporadic-E cloud is exactly 0.6 km in vertical extent. To estimate the thickness of the layer this study draws from the work of Zeng and Sokolovskiy (2010). The TEC values calculated in Section 3.4 are used for this technique, only the effective path length through the sporadic-E layer is changed. Both TEC methods provide the same height data points.

3.5.1 TEC with Variable Thickness Methods

Zeng and Sokolovskiy (2010) ran simulations of a tilted sporadic-E cloud showing a characteristic u-shape in the SNR amplitude as a function of altitude as the signal passes through the cloud. The tilt of the cloud with respect to the direction of propagation diminishes the effect of the cloud on the amplitude variation. In short, the signal is less changed the more perpendicular its path is with the sporadic-E cloud. For the purpose of this study, the angle is assumed to be zero in all cases. The location of the u-shape in the signal amplitude is designed as a comparison of the SNR smoothed over a 1 km window and the SNR smoothed over 20 km. The sporadic-E cloud is defined as the length between two 95% values of the 1 km smoothing compared to the 20 km average. For example, if the 20 km SNR average is 2, then the beginning of the layer would be when the 1 km average is 1.9, it would decrease below 1.9 and then rise again to 1.9. The sporadic-E layer thickness is the altitude difference between the two altitudes corresponding an SNR of 1.9. Zeng and Sokolovskiy (2010) found that the thickness of the sporadic-E clouds should be between 0.6-2 km.

Implementation of an automated process for comparison of the 1 km SNR and 20 km SNR averages with a minimum between proves difficult for the wide variation in measured SNR patterns. For this purpose, visual inspection of a similar process was executed to find the proper bounds of the u-shape for each of the 65 cases. Figure 25 illustrates an example of the characteristic u-shape in the normalized SNR of the L1 GPS signal.

Near the 105 km altitude there is an apparent u-shape in the normalized SNR data. To determine the layer thickness, the associated heights of the 95% values of the max SNR values with the thickest extent were used. This thickness is then used as the ΔR in Equation 11, redefining the geometry of the tube attributed to the TEC

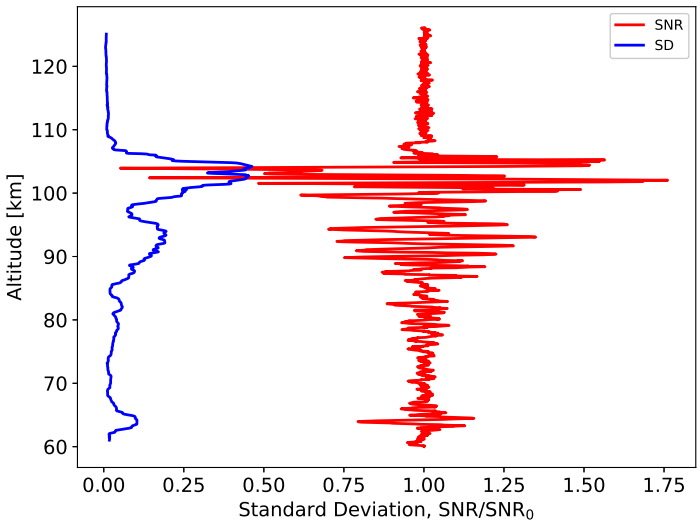

Figure 25. Standard deviation and normalized SNR for the L1 GPS signal as a function of altitude. The characteristic u-shape described by Zeng and Sokolovskiy (2010) is present near 105 km.

values. The largest of the thicknesses is 4.0 km which is double the estimated values from Zeng and Sokolovskiy (2010), and the smallest thickness is 1.3 km. The average of all the 65 thicknesses is 2.4 km, which is greater than the predicted values from Zeng and Sokolovskiy (2010). That maps to a path length of approximately 350 km which is much greater than the 176 km that the constant thickness approximately yields.

Figure 26 and Figure 27 demonstrate the large differences of the TEC with variable thickness technique as compared with the constant thickness. The thicknesses are much greater than the estimated thickness expected in the Zeng and Sokolovskiy (2010) research. Also, the path lengths in Figure 27 are on average double the length of constant thickness estimated path length of 176 km. These large differences indicate that the geometry assumptions in Hocke et al. (2001) seem to not be as accurate as preferred.

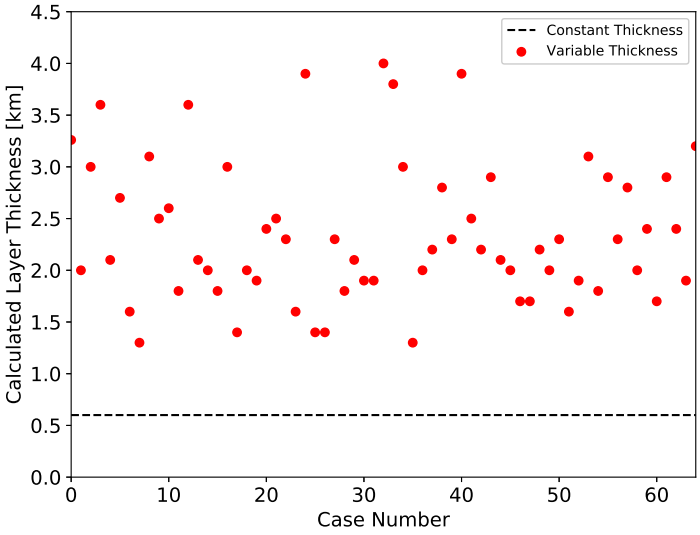

Figure 26. The calculated layer thickness using the TEC with variable thickness technique.

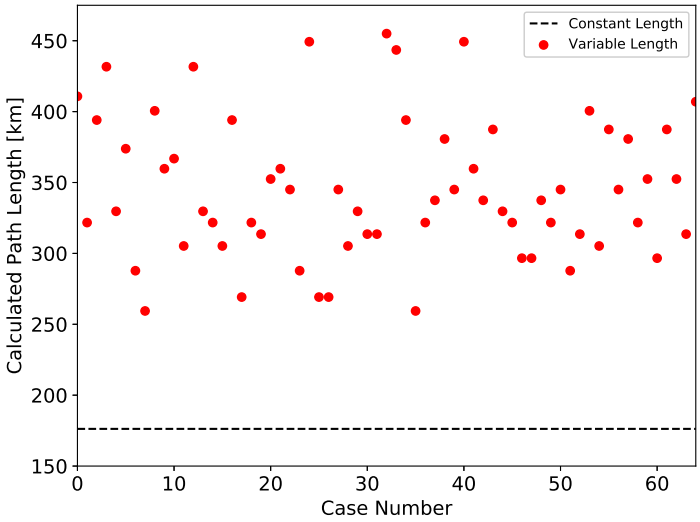

Figure 27. The calculated path length using the TEC with variable thickness technique.

3.5.2 TEC with Variable Thickness Results

A comparison of the fbEs predicted using the variable thickness TEC technique and the Digisonde observations is displayed in Figure 28. This technique underestimates the sporadic-E intensity, which is an artifact of the large path lengths calculated

using the variable thickness and the tube geometry outlined in (Hocke et al., 2001). Figure 29 shows the case by case error in the calculated fbEs values and highlights some of the large discrepancies. The largest error recorded through this method is -3.82 MHz, and the most accurate has an error of -0.05 MHz. There are 34 data points with errors larger than 1 MHz of error, and 3 points with absolute errors greater than 3 MHz.

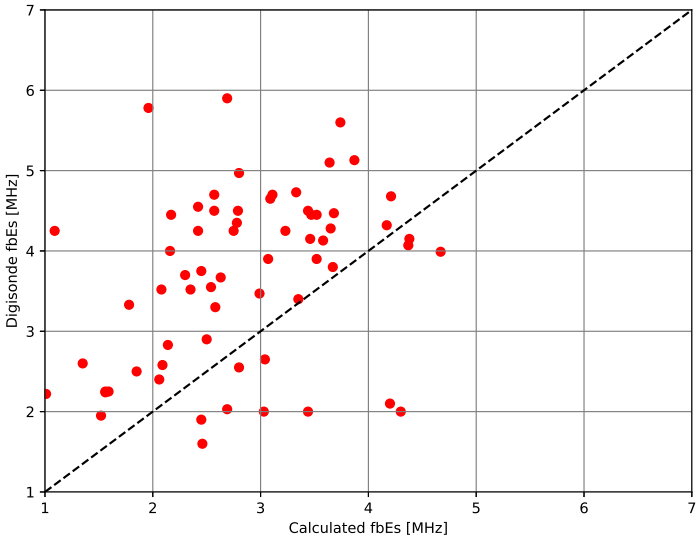

Figure 28. The TEC with variable thickness calculated fbEs compared to the Digisonde fbEs observation, with the dashed line as a perfect relationship.

Table 5. The average, standard deviation, root mean square error (RMSE), mean absolute error (MAE), relative mean absolute error (RMAE), and r^2 values for the comparison between the Digisonde fbEs values and the fbEs values for the TEC with variable thickness fbEs calculation technique. The error values have units of MHz.

Method	Avg	Std Dev	RMSE	MAE	RMAE	r^2
TEC w/ var ΔR	2.84	0.85	1.40	1.16	0.33	0.12
Digisonde	3.67	1.07	N/A	N/A	N/A	N/A

The statistics of this comparison are displayed in Table 5, which shows that this method underestimates the fbEs values by 0.8 MHz on average. The TEC with variable thickness method also shows less variation in the fbEs than the Digisonde

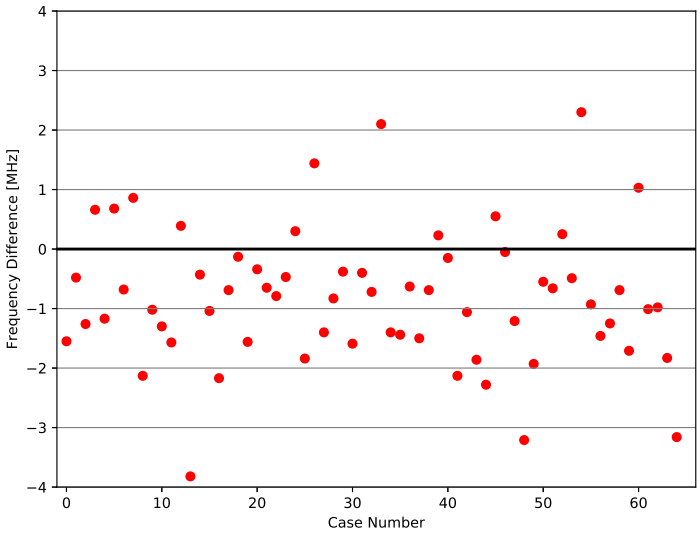

Figure 29. The difference between the observed Digisonde fbEs value and the calculated fbEs for each case using the TEC with variable thickness method.

measurements. While this technique removes the large errors observed for small fbEs estimated from the constant thickness technique (Figure 21), the average fbEs is reduced too far causing the overall agreement with the Digisonde data to decline. The variable thickness implemented in the tube geometry described in (Ahmad, 1998) provides sporadic-E tube lengths that are too large. This indicates that the assumption of a tube length strictly dependent on the thickness of the tube does not apply for sporadic-E clouds.

3.6 Frequency and Height Calculation Using Abel Transform

The three methods for frequency calculations and two methods for height estimates up to this point have been based on 65 case studies using the atmPhs files from CDACC. These files do not contain the necessary information for the Abel Transform implementation. This lead to a shrinking number of cases constrained by the available ionPrf files from the 65 cases for the other methods. Availability was limited to 22 cases in assessment of the Abel Transform. For this reason, those same

cases of the other methods will be used for comparison in later discussions.

3.6.1 Abel Transform Methods

The Abel transform is an inversion technique that can be applied to TEC profiles to obtain an electron density as a function of altitude (Ahmad, 1998; Hajj and Romans, 1998; Schriener et al., 1999). Previous studies using Abel transforms on GPS-RO data were performed prior to the launch of the COSMIC constellation, and we have not been able to find an application of the Abel transform to sporadic-E measurements in the literature. The Abel transform utilizes the ionPrf file type from CDAAC that only has a sample rate of 1 Hz making it much lower resolution than the GPS radio occultation data used from the previous three methods. These ionPrf files are used instead of atmPhs files because a complete TEC profile as a function of altitude (up to the altitude of the LEO satellite) is required for an accurate Abel transform. A fundamental assumption used in the Abel transform is that the ionosphere is spherically symmetric in the path of the GPS-RO signal. This assumption is inherently incorrect when a sporadic-E layer is present, but the technique is applied to analyze the impact of breaking this assumption. The TEC and electron density at an altitude R_0 can be described by

$$\tilde{T}(R_0) = 2\int_{R_0}^{R_{LEO}} \frac{R\,N(R)}{\sqrt{R^2 - R_0^2}}\,\mathrm{d}R \tag{12}$$

$$N(R) = -\frac{1}{\pi}\int_{R}^{R_{LEO}} \frac{\mathrm{d}\tilde{T}\Big/\mathrm{d}R_0}{\sqrt{R_0^2 - R^2}}\,\mathrm{d}R_0 \tag{13}$$

where $\tilde{T}$ is the TEC as a function of radial distance (altitude), R_{LEO} is the radial distance to the LEO satellite, R is the radius of interest, R_0 is a straight-line impact parameter, and N is the electron density at each altitude (Schriener et al., 1999). To

remove the discontinuity from the integral at the point $R = R_0$, and intermediate altitude R_{int} is selected slightly above R, and integration by parts provides

$$N(R) = -\frac{1}{\pi}\int_{R_{int}}^{R_{LEO}} \frac{\mathrm{d}\tilde{T}\Big/\mathrm{d}R_0}{\sqrt{R_0^2 - R^2}}\,\mathrm{d}R_0 - \frac{1}{\pi}\left[\left.\frac{\mathrm{d}\tilde{T}}{\mathrm{d}R_0}\right|_{R_{int}} \ln\left(\frac{R_{int}}{R} + \sqrt{\left(\frac{R_{int}}{R}\right)^2 - 1}\right)\right. \tag{14}$$

$$\left. - \int_R^{R_{int}} \frac{\mathrm{d}^2\tilde{T}}{\mathrm{d}R_0^2} \ln\left(\frac{R_0}{R} + \sqrt{\left(\frac{R_0}{R}\right)^2 - 1}\right)\mathrm{d}R_0\right].$$

Uncalibrated TEC measurements are used in this analysis, following the results of Schriener et al. (1999) which show a noticeable but relatively small difference in the electron density obtained from the calibrated TEC compared to the uncalibrated data. Numerical derivatives of the TEC provide the derivative terms, where the step size and corresponding grid as a function of altitude is controlled by the ionPrf resolution. A trapezoidal rule is used for integrating Equation 14. The CDAAC file also provided a full profile using an onion-peeling technique, a calculation of electron density layer by layer from the top of the atmosphere (Syndergaard et al., 2005). This technique is similar to the Abel transform technique, but uses quasi-calibrated TEC. This data from CDAAC was able to be used as a check to ensure the Abel transform technique wasn't too outlandish.

Figure 30 shows an example of an electron density profile obtained from the Abel transform. This full profile is useful to see the current state of the entire ionosphere, but a zoom into the E-layer required to analyze sporadic-E. Figure 31 shows the course resolution from the 1 Hz ionPrf files. Also, it demonstrates some of the limitations of the Abel transform technique using these ionPrf files with the lowest bound of the data near 100 km where the other techniques were able to be extended down into the 60 km range. However, this figure shows a sporadic-E layer near the 105 km altitude

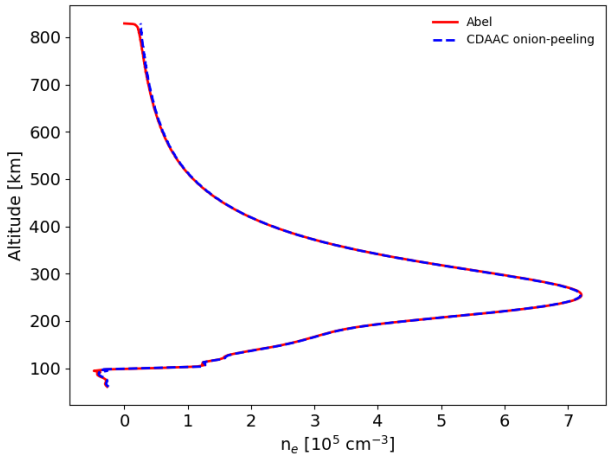

Figure 30. Vertical profile for the Abel transform in electron density space including the CDAAC full profile technique using onion-peeling.

of approximately 3.5 MHz. Almost all of the profiles for this comparison data set have similar profiles with just a small peak in the E-region.

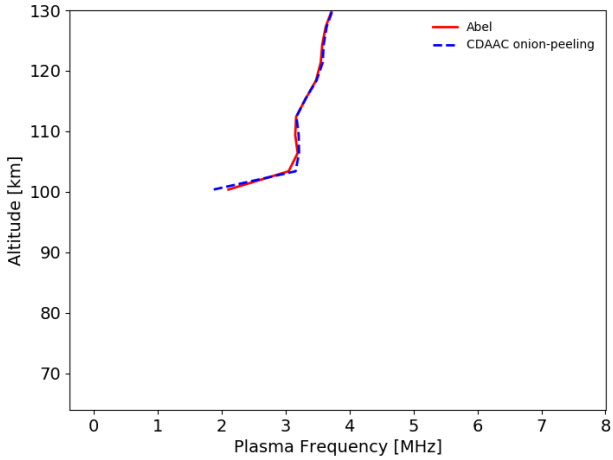

Figure 31. E-Layer profile for the Abel transform in plasma frequency space including the CDAAC profile technique using onion-peeling.

3.6.2 Abel Transform Results

The fbEs values calculated using an Abel transform are compared to the Digisonde measured values in Figure 32. Only 22 cases provided ionPrf files, which limits the number of data points for comparison. For these 22 cases, the Abel transform performs fairly well. Figure 33 shows the case by case error in the calculated fbEs values and highlights some of the large discrepancies. The largest error recorded through this method is -2.42 MHz, and the most accurate calculated value has an error of only -0.02 MHz.

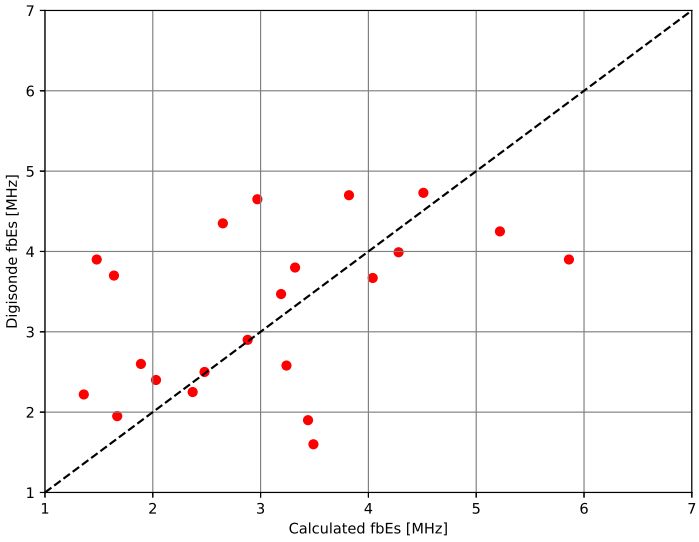

Figure 32. The calculated fbEs compared to the Digisonde fbEs observation for the Abel transform method, with the dashed line as a perfect relationship.

Table 6. The average, standard deviation, root mean square error (RMSE), mean absolute error (MAE), relative mean absolute error (RMAE), and r^2 values for the comparison between the Digisonde fbEs values and the fbEs values for the Abel transform fbEs calculation technique. The error values have units of MHz.

Method	Avg	Std Dev	RMSE	MAE	RMAE	r^2
Abel	3.27	1.18	1.16	0.90	0.30	0.20
Digisonde	3.08	0.98	N/A	N/A	N/A	N/A

Table 6 provides insight into the effectiveness of this technique for estimating

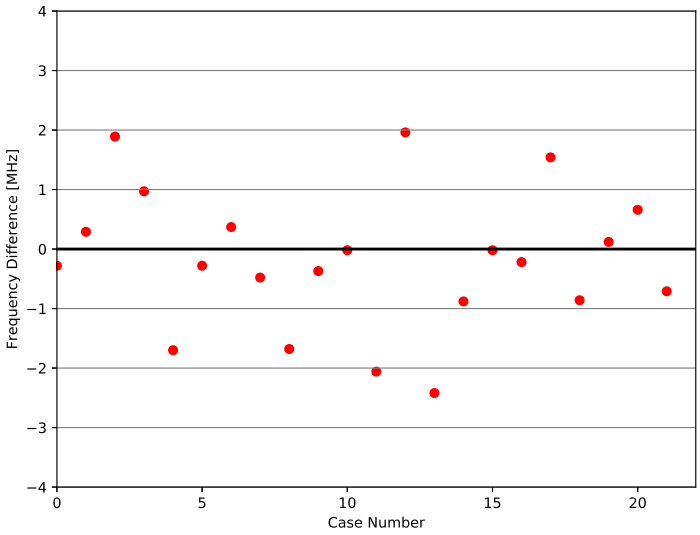

Figure 33. The difference between the observed Digisonde fbEs value and the calculated fbEs for each case using the Abel transform method.

sporadic-E intensity. The Abel transform overestimates the fbEs values on average by 0.2 MHz. There is also 0.2 MHz more spread in the Abel fbEs values shown by the standard deviation. There is a medium strength correlation between the two data sets illustrated by an r^2 of 0.2. While the Abel transform technique shows a decent fbEs comparison to the Digisonde measurements, it is important to compare them to the other three methods using the same data points, which is performed later in this chapter.

The Abel transform calculated heights are displayed with the Digisonde derived real heights in Figure 34. Similar to the intensity estimations, the calculated heights perform fairly well for these 22 cases. Figure 35 shows the case by case error in the calculated heights and highlights some of the large discrepancies. The largest error recorded through this method was -16.4 km. Overall, there is a bias for underestimating the height of the fbEs layer in the ionosphere, similar to the other techniques.

Table 7 shows the statics for this height comparison. The Abel transform underestimates the altitude by 1.6 km on average, and shows a 2.6 km larger spread than

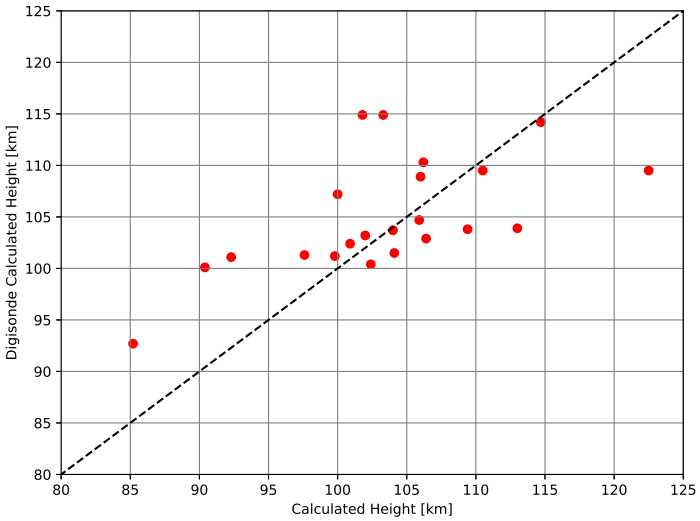

Figure 34. The Abel transform method calculated height compared to the Digisonde calculated height with the dashed line as a perfect relationship.

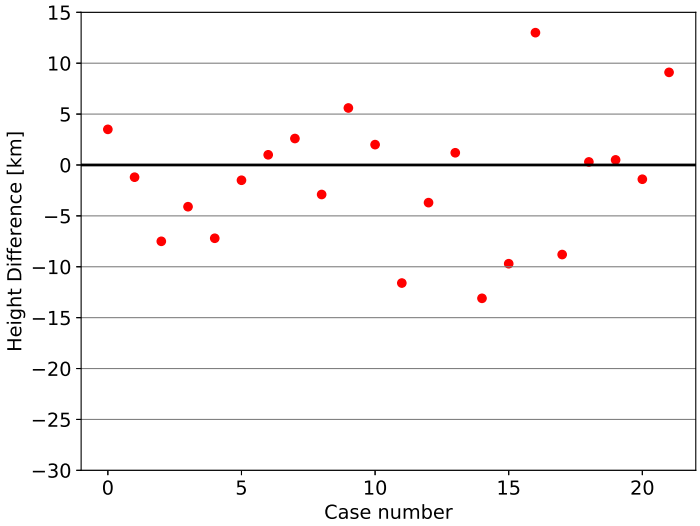

Figure 35. The difference between the calculated Digisonde height and the Abel transform calculated height for each case.

the Digisonde data. The r^2 value indicates that there is a strong correlation between the Abel transform predicted heights and the Digisonde heights. More analysis of the effectiveness of the Abel transform method is provided in the comparison between each method in the next section.

Table 7. The average, standard deviation, root mean square error (RMSE), mean absolute error (MAE), relative mean absolute error (RMAE), and r^2 values for the comparison between the Digisonde calculated heights and the determined heights for the Abel transform height calculation technique. The error values have units of km.

Method	Avg	Std Dev	RMSE	MAE	RMAE	r^2
Abel	103.6	8.0	6.5	5.1	0.05	0.37
Digisonde	105.1	5.4	N/A	N/A	N/A	N/A

3.7 Technique Comparisons

The results thus far have been presented independently, but this sections provides a combined comparison to analyze the relative accuracy of each technique. First the 65 cases for the S4, TEC with constant thickness, and TEC with variable thickness methodologies are analyzed. Then the appropriate 22 cases of those three methods will be compared with the Abel transform technique.

3.7.1 Technique Comparison: 65 cases

This section combines the S4, TEC with constant thickness and TEC with variable thickness methods into a single data set for comparison. This combination includes the 65 cases for each of these techniques across the globe.

Figure 36 shows the combination of the S4, TEC with constant thickness and TEC with variable thickness methods compared to the Digisonde fbEs observations, and illustrates where each of the techniques show weakness at matching the Digisonde observations. For instance, none of the methods are particularly adept at matching the observations for the strongest fbEs events of greater than 5 MHz. The TEC with constant thickness performs the best in this region, but all of the methods have instances of very large errors when attempting to predict large fbEs magnitudes. Also, none of the techniques accurately predict the weaker fbEs events of 2 MHz or less, with many of the large differences in that region.

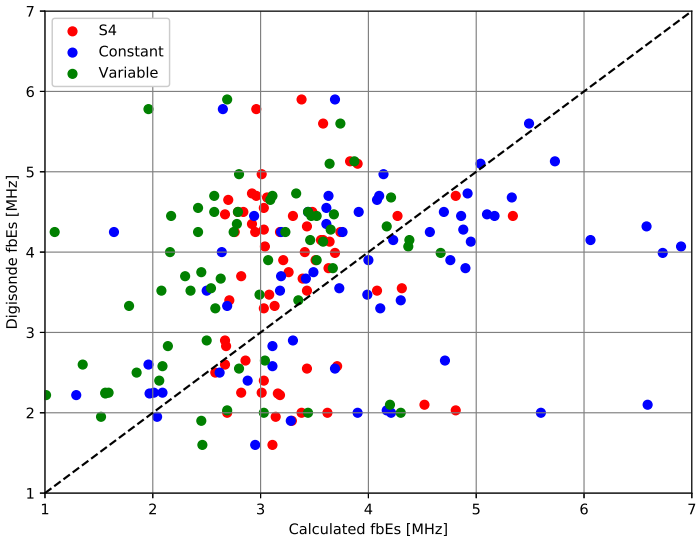

Figure 36. The calculated fbEs values compared to the Digisonde fbEs observations for the S4, TEC with constant thickness and TEC with variable thickness methods, with the dashed line as a perfect relationship.

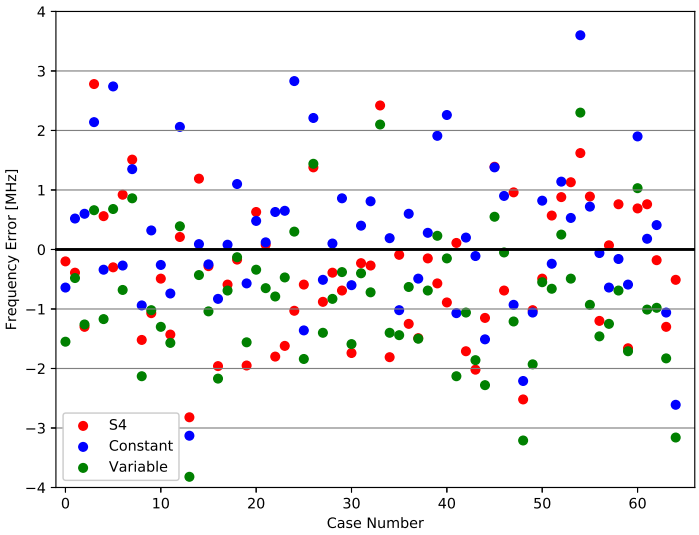

Figure 37. The difference between the observed Digisonde fbEs value and the calculated fbEs for the S4, TEC with constant thickness and TEC with variable thickness for each case.

Figure 37 shows the case by case fbEs errors for each of the techniques, and highlights the variability in the techniques. Both the S4 calculation and the TEC with variable thickness have similar groupings in Figure 36 and Figure 37, and consistently

underestimate the fbEs. However, the TEC with variable thickness follows the expected pattern along the dashed line slightly more than the S4 method. The TEC with constant thickness follows the expected trend better than both the other techniques, but has some very large differences on a few of the cases. A majority of the TEC with constant thickness points have relatively low errors, as shown in Figure 37.

Table 8. The average, standard deviation, root mean square error (RMSE), mean absolute error (MAE), relative mean absolute error (RMAE), and r^2 values for the comparison between the Digisonde fbEs values and the fbEs values for each technique. The error values have units of MHz.

Method	Avg	Std Dev	RMSE	MAE	RMAE	r^2
S4	3.32	0.56	1.23	1.01	0.30	0.01
TEC w/ con ΔR	3.94	1.27	1.38	1.01	0.33	0.12
TEC w/ var ΔR	2.84	0.85	1.40	1.16	0.33	0.12
Digisonde	3.67	1.07	N/A	N/A	N/A	N/A

Table 8 combines all the previously outlined statistics for the three methods used in this comparison. The S4 and TEC with variable thickness both underestimate the fbEs, but the variable thickness method is 0.8 MHz below the Digisonde average while the S4 method is only 0.4 MHz below. The TEC with constant thickness has the closest average, with an overestimation of 0.3 MHz. Also, the S4 and TEC with variable thickness have tighter groupings of the data while the TEC with constant thickness is more variable as indicated by the standard deviations. The r^2 shows that the two TEC methods show approximately the same moderate correlation between the estimates and the Digisonde fbEs values while the S4 method is poorly correlated. While the TEC methods show the most correlated, the errors tell a different story with the the S4 having the lowest errors across the board. The TEC with constant thickness is between the two others on the error measures, with the TEC with variable thickness having the largest errors. Overall, none of the methods shine as the most accurate or as a perfect technique for comparison to the Digisonde fbEs values.

The heights calculated for the same data set are compared to the Digisonde de-

rived actual heights in Figure 38. Both the TEC techniques perform well around their averages in the 100-110 km, but do not handle the lower and higher heights as measured by the Digisondes. The S4 technique however appears to show a more consistent grouping along the expected correlation line.

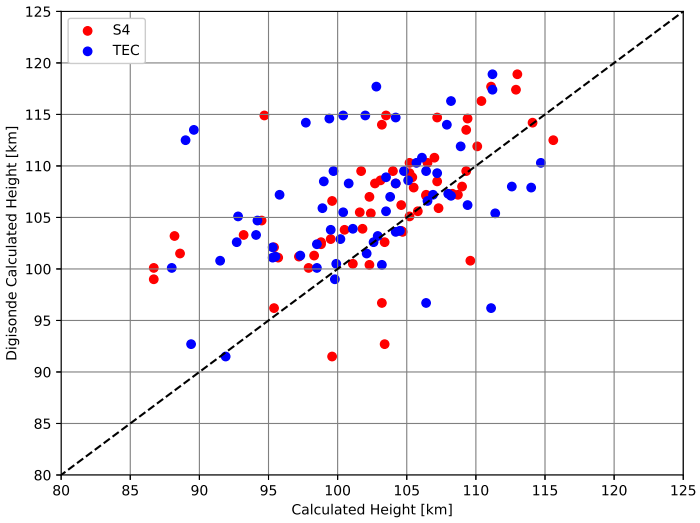

Figure 38. The calculated fbEs height compared to the Digisonde calculated height with the dashed line as a perfect relationship.

Figure 39 illustrates the combination of the S4 and TEC height differences with respect to the Digisonde actual heights and shows the overall underestimation of the techniques. The TEC method has more absolute differences greater than 10 km than the S4 method. There also isn't a dependence by case for the difference, meaning that the TEC performs better on some cases and S4 on others. This implies that the techniques provide independent results.

Table 9 demonstrates the combination of the statistics for the S4 and TEC height calculations and shows the underestimation bias across the board. Also, the similarity of the standard deviation values helps illustrate that there is some ability for the two methods to capture the spread in the height measurements. Using the r^2 values, S4 is shown for have a much stronger correlation for the height calculations. The S4 also

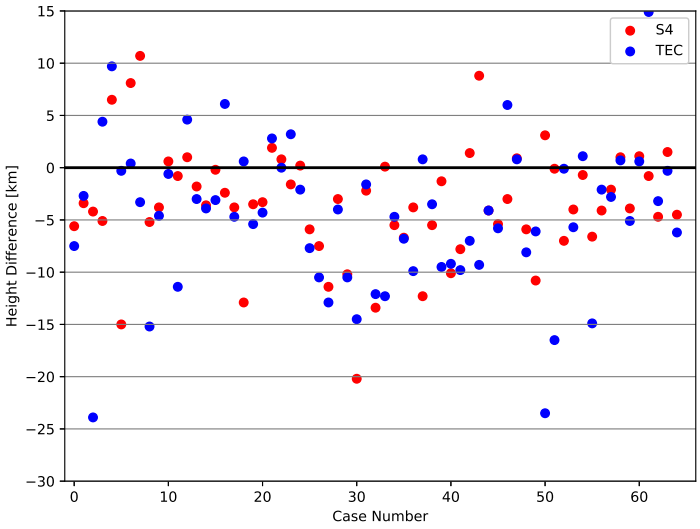

Figure 39. The difference between the calculated Digisonde height and estimated height for each case.

Table 9. The average, standard deviation, root mean square error (RMSE), mean absolute error (MAE), relative mean absolute error (RMAE), and r^2 values for the comparison between the Digisonde calculated heights and the determined heights for each technique. The error values have units of km.

Method	Avg	Std Dev	RMSE	MAE	RMAE	r^2
S4	103.0	6.3	6.4	4.9	0.05	0.37
TEC	101.9	6.4	8.3	6.4	0.06	0.14
Digisonde	106.5	5.8	N/A	N/A	N/A	N/A

has much lower errors across the board than the TEC model further demonstrating that overall, the S4 technique is better than the TEC method for accurately assessing the height of the sporadic-E layers.

Between the fbEs and height calculations, none of the methods shines as more capable of accurately assessing the fbEs and heights of the sporadic-E layers. The two TEC methods are more correlated to the fbEs values measured by the Digisondes, but still show large differences on average and the only moderate strength correlations. Though the TEC methods have much worse errors than the S4 method in the fbEs comparison. The S4 technique shows almost no correlation to the Digisonde fbEs

values, but is much better at assessing the height of the layers than the TEC method, across all measures. To this point, the assessment has been been restricted to the 65 cases and excluded the Abel transform technique due to the difference in the data sets. Next the Abel transform will be compared to the corresponding cases using the other three methods.

3.7.2 Technique Comparison: 22 cases

This section combines the fbEs calculations for the S4, TEC with constant thickness, TEC with variable thickness, and Abel transform methods into a comparison for the appropriate 22 cases. Due to the smaller data set, conclusions from this analysis will be weaker than those previously outlined in the last section.

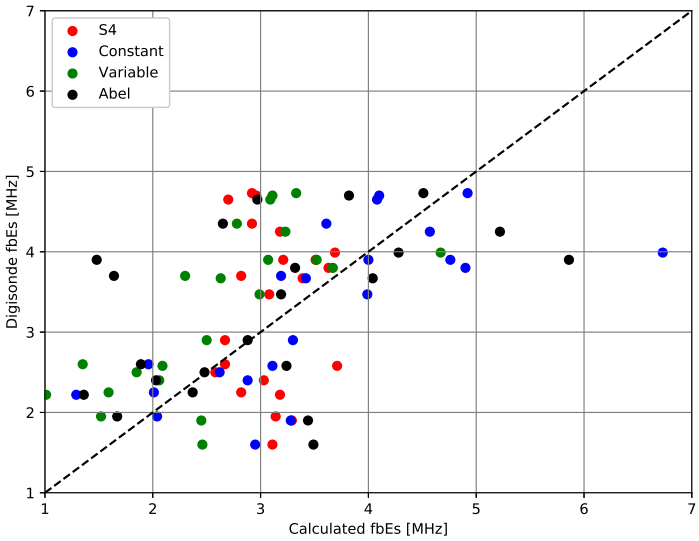

Figure 40. The calculated fbEs values compared to the Digisonde fbEs observation with the dashed line as a perfect relationship.

Figure 40 illustrates the combination of the 22 cases for the S4, TEC with constant thickness, and TEC with variable thickness with the Abel transform compared with the Digisonde fbEs. None of the techniques show a tight grouping to the dashed line

for this data set. One defining difference of this comparison is the elimination of the strongest fbEs events of greater than 5 MHz from the larger number of 65 cases. Because of this absence, all of the methods appear to perform well for the intensity estimations. However, the inclusion of the stronger fbEs events would provide a better test of the different methods, and limited conclusions can be drawn from this small data set.

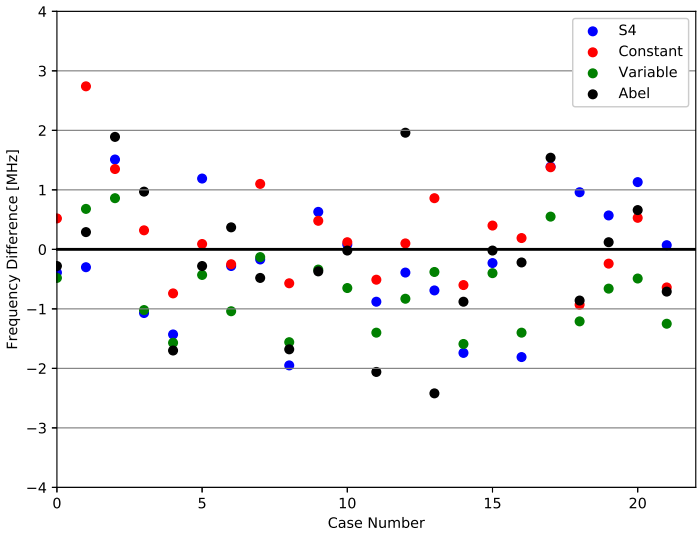

Figure 41. The difference between the observed Digisonde fbEs value and the calculated fbEs for each case.

Figure 41 demonstrates the small differences between the techniques and the Digisonde fbEs values with a majority of all the methods having less than 1 MHz differences. The Abel transform has the third most differences of greater than 1 MHz behind the S4 method and TEC with variable thickness with a majority of the fbEs values underestimating the expected Digisonde fbEs values. The Abel transform has 7 points with greater than 1 MHz difference, S4 has 8 points, TEC with constant thickness has 4 points, and TEC with variable thickness has 9 points.

At first glance Table 10 makes the S4 technique look like it performs well for fbEs on this data set, but the small variation of the S4 calculations and the poor r^2

Table 10. The average, standard deviation, root mean square error (RMSE), mean absolute error (MAE), relative mean absolute error (RMAE), and r^2 values for the comparison between the Digisonde fbEs values and the fbEs values for each technique. The error values have units of MHz.

Method	Avg	Std Dev	RMSE	MAE	RMAE	r^2
S4	3.10	0.33	1.04	0.86	0.29	0.00
TEC w/ con ΔR	3.53	1.20	0.88	0.67	0.23	0.52
TEC w/ var ΔR	2.60	0.84	0.97	0.86	0.27	0.51
Abel	3.27	1.18	1.16	0.90	0.30	0.20
Digisonde	3.08	0.98	N/A	N/A	N/A	N/A

show that this technique tends to group the predicted fbEs values in a small window. Both of the TEC methods show strong correlations with the Digisonde data with the highest r^2 values. The TEC methods have the lowest errors through this data set with the TEC with constant thickness outperforming the rest. By comparison, the Abel method does well on average and has a similar spread to the data, but it doesn't correlate to the Digisonde as strongly as the TEC methods and is the worst method in the error analysis. Overall, in the more limited data set for the fbEs the TEC methods that try to capture the physical nature of the sporadic-E events perform better.

Figure 42 shows the combination of the S4, TEC and Abel height calculation techniques compared to the Digisonde derived actual heights. It highlights similar results as the S4 and TEC comparison in the previous section where the methods perform well around their averages, but have trouble predicting altitudes on the high and low extremes. Figure 43 highlights the same underestimation bias of the methods compared to the Digisonde calculated heights. It shows that the majority of the data points are within 5 km of the measured heights, but there are some large outliers that drag the accuracy down.

Table 11 shows that the Abel transform appears to be the best method for height calculations on this data set. The average is the closest to the Digisonde average with

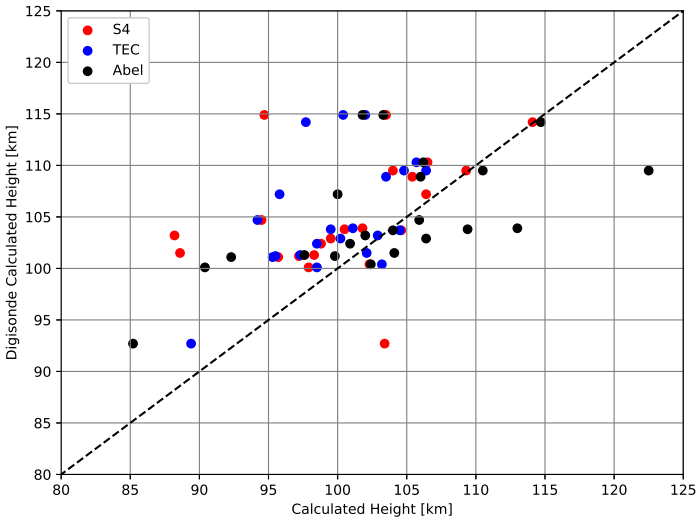

Figure 42. The calculated fbEs height compared to the Digisonde calculated height with the dashed line as a perfect relationship.

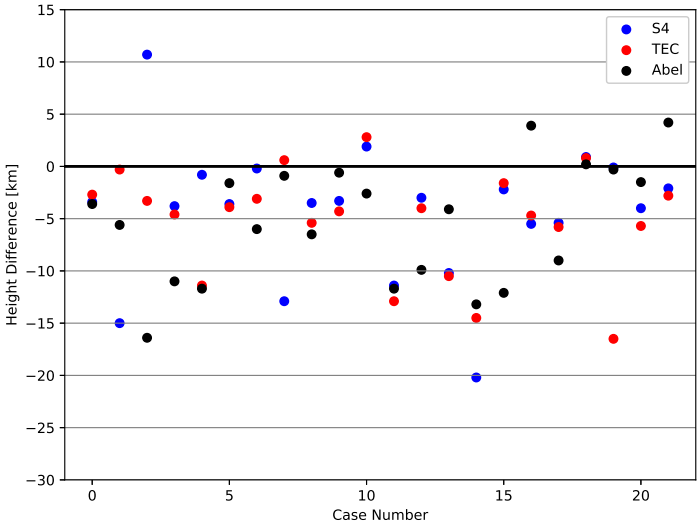

Figure 43. The difference between the calculated Digisonde height and estimated height for each case.

a 1.5 km difference. Also, the Abel transform has the strongest correlation compared to the other methods. The only detraction is the larger spread of the data with a 2.6 km increase in the standard deviation compared to the Digisonde data. However, the errors are smaller than the S4 or TEC techniques. The S4 and TEC methods perform

Table 11. The average, standard deviation, root mean square error (RMSE), mean absolute error (MAE), relative mean absolute error (RMAE), and r^2 values for the comparison between the Digisonde calculated heights and the determined heights for each technique. The error values have units of km.

Method	Avg	Std Dev	RMSE	MAE	RMAE	r^2
S4	100.7	6.1	7.7	5.6	0.05	0.16
TEC	99.9	4.2	7.1	5.6	0.05	0.24
Abel	103.6	8.0	6.5	5.1	0.05	0.37
Digisonde	105.1	5.4	N/A	N/A	N/A	N/A

about the same in this analysis with a slightly stronger correlation for the TEC than the S4 height method.

Overall, the lower resolution data for the Abel transform is able to capture the heights of the sporadic-E layers, but isn't as accurate in the analysis of the fbEs. This may be caused by a combination of the lower resolution data used to perform the Abel transforms in addition to the deviation from the assumption of spherical symmetry. High resolution ionosphere data expected from COSMIC-II should be used to repeat this analysis to test the effect of temporal resolution on the accuracy of the sporadic-E intensity estimations. The methods that attempt to capture the physical nature of the ionosphere, the Abel transform and the two TEC methods, are better at capturing the fbEs and heights compared to the Digisonde measurements. No method truly shines as an easily implementable and accurate on both the fbEs and height measurements, but a potentially higher resolution Abel transform technique could prove more effective if the proper data set existed.

IV. Conclusions

This study analyzed the performance of GPS radio occultation techniques used to measure sporadic-E intensity and height by comparing to ground based ionosonde measurements on a global scale. Four different techniques to calculate sporadic-E intensity in terms of an fbEs were analyzed for this study: SNR S4, TEC with constant thickness, TEC with variable thickness, and an Abel transform. These GPS-RO methods were compared to Digisonde measurements, within 150 km and 30 minutes of each other, across the globe for the years 2010 and 2014 using data from the GIRO network, and the Digisonde measurements were taken as the true intensity and height. Digisonde measured virtual heights were converted to actual heights by using ionogram derived electron density profiles. With the goal of selecting a single method to implement for near real-time global observations, the difficulty of depicting the wide range of sporadic-E configurations using remote sensing observations was demonstrated. While the different techniques show problems predicting the fbEs and height for the entire data set, each of the techniques have their own strengths and weaknesses.

The linear relationship between S4 and fbEs used in this analysis showed a tendency to group the fbEs estimates between 3-4 MHz while the Digisonde measurements showed a much larger spread. This grouping is most likely an artifact of the limited data set used to derive the linear relationship which contained fbEs values in this range. While S4 performed well in this region, it was very poor at handling the strongest layers of greater than 5.0 MHz and the weakest layers of less than 2.5 MHz, predominantly trying to fit those cases into the region of 3-4 MHz where it performed well. The grouping of this data did lead to the best performance across the error metrics for the S4 on the large data set. This inaccurate depiction of the events really

was demonstrated by the almost random correlation between the S4 calculated values and the Digisonde fbEs observations with an r^2 value of nearly zero, indicating a potentially nonlinear relationship between S4 and fbEs that should be explored with a larger data set. Additionally, the orientation of the sporadic-E layer is known to affect the magnitude of scintillation, and should be taken into account when determining the relationship between S4 and fbEs. While the characterization of the strength of the fbEs by the S4 method was tenuous at best, the height estimates were better with an average underestimation of 3.5 km and an r^2 value of 0.4. The S4 height calculations performed best in the middle of the altitude range near 103 km. The S4 method performed better than the TEC techniques with respect to predicting the height of the sporadic-E layers. From an implementation perspective the S4 method is very straightforward and easily repeatable, which provides an advantage over the other techniques.

The TEC with constant thickness technique showed more ability to accurately assess the sporadic-E fbEs values across the range of the events. The r^2 value of 0.1 is much better than the S4 method, and there isn't a noticeable bias to a particular range of intensities. On average, the intensities are overestimated by 0.3 MHz using this technique. The errors are not quite as good as the S4 technique, but the RMAE is similar in value indicating in a relative sense the methods are almost as accurate. The data has a wider spread similar to that of the Digisonde observations, but some of the assumptions that went into the calculation of the TEC are preventing this method from being more accurate. The constant thickness of 0.6 km assumed for the sporadic-E layer in comparison to the measured thicknesses show that this assumption is unphysical. Additionally, the orientation of the clouds with respect to the GPS-RO signal path are unknown, which significantly affects the TEC to electron density conversion.

The TEC with variable thickness technique has the same r^2 value as the constant thickness method, but underestimates the strength of the layer by 0.8 MHz on average. Also, the errors for the TEC with variable thickness are the worst of the three methods for the fbEs comparison. The tube geometry assumed for this variable thickness method assumes that the sporadic-E width depends on the thickness. From these results, this does not appear to be the case, and the tube geometry assumption is incomplete for use in sporadic-E calculations. The height calculations from the TEC technique underestimate the heights by 4.6 km on average, and the correlation is weaker than the S4 method. While the TEC height calculations performed better near the average altitude, they were poor at predicting altitudes above 110 km. The dependence of the TEC results on the detrending technique requires additional research to determine the most appropriate detrending technique for monitoring sporadic-E.

On the smaller data set of 22 points used for comparison with the Abel transform technique, the Abel transform overestimates the strength of the fbEs events by 0.2 MHz and shows a medium strength correlation to the Digisonde measurements with an r^2 value of 0.2. Though this seems the best compared to the larger data set, the TEC methods on the same data set show stronger correlations of $r^2 \approx 0.5$. The Abel transform is more accurate on average, but that difference in correlation highlights the effectiveness of the TEC values. For this limited data set, the S4 intensities are still uncorrelated to the Digisonde observations. The height estimates from the Abel transform perform the best for this limited data set with an average underestimation of 1.5 km and a correlation of 0.4. This demonstrates the Abel transform's ability to detect the location of the sporadic-E events, but the coarseness of the temporal data resolution severely limits the capability of accurately measuring the strength of the fbEs. With the upcoming launch of COSMIC-II, a higher resolution data set for the ionosphere may increase the accuracy of the intensity estimations from the Abel

transform.

Overall, the three methods grounded in the physical representation of the ionosphere of the TEC with constant thickness, TEC with variable thickness and Abel transform described the strength of the sporadic-E events better than the empirical S4 method. The two TEC methods appear to have the perform the best on predicting sporadic-E intensities, but both have room for improvement. A lack of an accurate sporadic-E width and orientation used in the conversion of TEC to electron density is the limiting factor for this technique, and more research is required to predict this thickness in near real-time. While some improvement is required to make these techniques both accurate and reliable for all sporadic-E configurations, they do provide quality estimations of the fbEs provided by the Digisonde observations. It must also be noted that differences in GPS-RO and Digisonde measured locations and times may be a major cause of disparities in the results, and the assumption that both types of measurements are monitoring the same position in the sporadic-E cloud may be faulty. An expansion of these methods to a more robust data set could provide more insight into the bias, limitations, and usefulness of each technique. Overall, some of the methods show promise for measuring the height and intensity of sporadic-E layers using GPS radio occultation measurements, and with further improvement could prove useful in global, near real-time maps of sporadic-E activity.

For further validation of this study's intent and application, an expansion on the 2 year data set to the full compliment of the CDAAC database and use of the DIDBase for those years through 2017 would lend credence to which methods should be implemented in the future. Additional techniques, such as radio holography, should also be explored as alternative methods for calculating sporadic-E intensity. Also, there are limited models that are able to simulate the existence of sporadic-E layers, because of the aforementioned chemistry complexity and neutral wind fields. A comparison of

the occurrence rates and locations between GPS-RO measured sporadic-E and model predictions would prove useful for model validation. Another modeling application would be for integration of these techniques into the model to determine if even with non-ideal fbEs estimates observations would be beneficial to the forecasts.

Bibliography

Ahmad, B. (1998). *Accuracy and resolution of atmospheric profiles obtained from radio occultation measurements. Scientific Rep.* PhD thesis.

Aikin, A. and Goldberg, R. (1973). Metallic ions in the equatorial ionosphere. *Journal of Geophysical Research*, 78(4):734–745.

Arras, C. (2010). A global survey of sporadic e layers based on gps radio occultations by champ, grace and formosat-3/cosmic.

Arras, C. and Wickert, J. (2018). Estimation of ionospheric sporadic e intensities from gps radio occultation measurements. *Journal of Atmospheric and Solar-Terrestrial Physics*, 171:60–63.

Arras, C., Wickert, J., Beyerle, G., Heise, S., Schmidt, T., and Jacobi, C. (2008). A global climatology of ionospheric irregularities derived from gps radio occultation. *Geophysical research letters*, 35(14).

Baggaley, W. (1984). Ionospheric sporadic-e parameters: long-term trends. *Science*, 225(4664):830–833.

Barnum, J. R. and Simpson, E. E. (1997). Over-the-horizon radar sensitivity enhancement by impulsive noise excision. In *Radar Conference, 1997., IEEE National*, pages 252–256. IEEE.

Bates, D. and Dalgarno, A. (1962). Electronic recombination. In *Pure and Applied Physics*, volume 13, pages 245–271. Elsevier.

Center, L. G. D. (2018). Global ionosphere radio observatory. `http://giro.uml.edu/`.

Chu, Y., Wang, C., Wu, K., Chen, K., Tzeng, K., Su, C., Feng, W., and Plane, J. (2014). Morphology of sporadic e layer retrieved from cosmic gps radio occultation measurements: Wind shear theory examination. *Journal of Geophysical Research: Space Physics*, 119(3):2117–2136.

Chu, Y.-H., Su, C.-L., and Ko, H.-T. (2010). A global survey of cosmic ionospheric peak electron density and its height: A comparison with ground-based ionosonde measurements. *Advances in Space Research*, 46(4):431–439.

Gurnett, D. A. and Bhattacharjee, A. (2005). *Introduction to plasma physics: with space and laboratory applications*. Cambridge university press.

Hajj, G. and Romans, L. (1998). Ionospheric electron density profiles obtained with global positioning system: Results from the gps/met experiment. *Radio Science*, 33(1):175–190.

Hines, C. (1964). The formation of midlatitude sporadic e layers. *Journal of Geophysical Research*, 69(5):1018–1019.

Hocke, K., Igarashi, K., Nakamura, M., Wilkinson, P., Wu, J., Pavelyev, A., Wickert, J., et al. (2001). Global sounding of sporadic e layers by the gps/met radio occultation experiment. *Journal of Atmospheric and Solar-Terrestrial Physics*, 63(18):1973–1980.

International, L. D. (2019). Didbase (digital ionogram database). `http://ulcar.uml.edu/DIDBase/`.

Maksyutin, S., Sherstyukov, O., and Fahrutdinova, A. (2001). Dependence of sporadic-e layer and lower thermosphere dynamics on solar activity. *Advances in Space Research*, 27(6-7):1265–1270.

Manucci, A., Iijima, B., Lindqwister, U., Pi, X., Sparks, L., and Wilson, B. (1999). Gps and ionosphere: Ursi reviews of radio science. *Jet Propulsion Laboratory, Pasadena*.

Mathews, J. (1998). Sporadic e: current views and recent progress. *Journal of atmospheric and solar-terrestrial physics*, 60(4):413–435.

Niu, J., Fang, H., Wang, X.-x., Weng, L., and Guo, L. (2015). Analysis of the ionosphere irregularities in e region based on cosmic occultation data. *Advances in Space Research*, 56(9):1895–1900.

Pavelyev, A., Tsuda, T., Igarashi, K., Liou, Y., and Hocke, K. (2003). Wave structures in the electron density profile in the ionospheric d-and e-layers observed by radio holography analysis of the gps/met radio occultation data. *Journal of atmospheric and solar-terrestrial physics*, 65(1):59–70.

Piggott, W. and Rawer, K. (1978). Ursi handbook of ionogram interpretation and reduction, 1961.

Pisacane, V. L. (2008). *The space environment and its effects on space systems*. American Institute of aeronautics and Astronautics.

Rishbeth, H. and Garriott, O. K. (1969). Introduction to ionospheric physics. *IEEE Transactions on Image Processing*, 1.

Schriener, W., Sokolovskiy, S., Rocken, C., and Hunt, D. (1999). Analysis and validation of gps/met radio occultation data in the ionosphere. *Radio Science*, 34(4):949–966.

Schunk, R. and Nagy, A. (2009). *Ionospheres: physics, plasma physics, and chemistry*. Cambridge university press.

Syndergaard, S., Kursinski, E. R., Herman, B. M., Lane, E. M., and Flittner, D. E. (2005). A refractive index mapping operator for assimilation of occultation data. *Monthly weather review*, 133(9):2650–2668.

UCAR (2019). Cdaac: Cosmic data analysis and archive center. `https://cdaac-www.cosmic.ucar.edu/`.

Van Dierendonck, A. and Arbesser-Rastburg, B. (2004). Measuring ionospheric scintillation in the equatorial region over africa, including measurements from sbas geostationary satellite signals. In *Proceeding of ION GNSS 17th technical meeting of the satellite division, Long Beach, CA*, volume 316.

Whitehead, J. (1961). The formation of the sporadic-e layer in the temperate zones. *Journal of Atmospheric and Terrestrial Physics*, 20(1):49–58.

Whitehead, J. (1989). Recent work on mid-latitude and equatorial sporadic-e. *Journal of Atmospheric and Terrestrial Physics*, 51(5):401–424.

Wickert, J., Pavelyev, A., Liou, Y., Schmidt, T., Reigber, C., Igarashi, K., Pavelyev, A., and Matyugov, S. (2004). Amplitude variations in gps signals as a possible indicator of ionospheric structures. *Geophysical research letters*, 31(24).

Wu, D. L., Ao, C. O., Hajj, G. A., de La Torre Juarez, M., and Mannucci, A. J. (2005). Sporadic e morphology from gps-champ radio occultation. *Journal of Geophysical Research: Space Physics*, 110(A1).

Yakovlev, O., Wickert, J., Pavelyev, A., Matyugov, S., and Anufriev, V. (2008). Sporadic structures in equatorial ionosphere as revealed from gps occultation data. *Acta Astronautica*, 63(11):1350–1359.

Yeh, W.-H., Huang, C.-Y., Hsiao, T.-Y., Chiu, T.-C., Lin, C.-H., and Liou, Y.-A.

(2012). Amplitude morphology of gps radio occultation data for sporadic-e layers. *Journal of Geophysical Research: Space Physics*, 117(A11).

Yue, X., Schreiner, W., Zeng, Z., Kuo, Y., and Xue, X. (2015). Case study on complex sporadic e layers observed by gps radio occultations. *Atmospheric Measurement Techniques*, 8(1):225–236.

Zeng, Z. and Sokolovskiy, S. (2010). Effect of sporadic e clouds on gps radio occultation signals. *Geophysical Research Letters*, 37(18).

REPORT DOCUMENTATION PAGE

Form Approved
OMB No. 0704–0188

1. REPORT DATE *(DD–MM–YYYY)*	2. REPORT TYPE	3. DATES COVERED *(From — To)*
01–07–2019	Master's Thesis	May 2017 — Mar 2019

4. TITLE AND SUBTITLE

GLOBAL IONOSONDE AND GPS RADIO OCCULTATION SPORADIC-E INTENSITY AND HEIGHT COMPARISON

5a. CONTRACT NUMBER

5b. GRANT NUMBER

5c. PROGRAM ELEMENT NUMBER

6. AUTHOR(S)

Gooch, Joshua Young, Capt, USAF

5d. PROJECT NUMBER

5e. TASK NUMBER

5f. WORK UNIT NUMBER

7. PERFORMING ORGANIZATION NAME(S) AND ADDRESS(ES)

Air Force Institute of Technology
Graduate School of Engineering and Management (AFIT/EN)
2950 Hobson Way
WPAFB OH 45433-7765

8. PERFORMING ORGANIZATION REPORT NUMBER

AFIT-ENP-MS-19-M-079

9. SPONSORING / MONITORING AGENCY NAME(S) AND ADDRESS(ES)

Air Force Research Laboratory/Space Vehicles
3550 Aberdeen Avenue SE
Kirtland AFB, NM 87117
DSN 246-3172, COMM 505-846-3172
Email: jonah.colman.1@us.af.mil

10. SPONSOR/MONITOR'S ACRONYM(S)

AFRL/RV

11. SPONSOR/MONITOR'S REPORT NUMBER(S)

12. DISTRIBUTION / AVAILABILITY STATEMENT

DISTRIBUTION STATEMENT A:

13. SUPPLEMENTARY NOTES

14. ABSTRACT

A global, multi-year comparison of low and mid-latitude COSMIC GPS radio occultation (RO) sporadic-E (E_s) plasma frequency and altitude and Digisonde blanketing frequency (fbEs) and altitude within 150 km and 30 minutes of each other. RO methods used to estimate the intensity of the E_s layer include the scintillation index S4, total electron content (TEC) with both a constant and variable E_s cloud thickness, and an Abel transform. The S4 and TEC with varying thickness techniques both under-represent the fbEs values while the TEC with constant thickness and Abel transform better estimate Digisonde fbEs values. All RO methods underestimate the altitude of the fbEs events as measured by the Digisondes. No method outperformed the other techniques across every metric, but the physical basis of the TEC technique provides an advantage over the empirically derived S4. The Abel transform also shows promise, but the lower resolution data currently available is detrimental to its performance. Overall, an automated TEC method tested on a larger data set could prove valuable for real-time global E_s observation.

15. SUBJECT TERMS

GPS Radio Occultation, Sporadic-E, Ionosphere

16. SECURITY CLASSIFICATION OF:			17. LIMITATION OF ABSTRACT	18. NUMBER OF PAGES	19a. NAME OF RESPONSIBLE PERSON
a. REPORT	b. ABSTRACT	c. THIS PAGE			Maj Daniel J. Emmons, AFIT/ENP
U	U	U	U	87	19b. TELEPHONE NUMBER *(include area code)* (937) 255-3636, x4571; Daniel.Emmons@afit.edu

Standard Form 298 (Rev. 8–98)
Prescribed by ANSI Std. Z39.18